MOLECULAR-SIZE EFFECTS OF POLY(ETHYLENE GLYCOL) DOXORUBICIN NANOCARRIERS ON THE INTRADUCTAL TREATMENT OF DUCTAL CARCINOMA IN SITU (DCIS)

By

ZICHAO GU

A dissertation submitted to the

Graduate School-New Brunswick

Rutgers, The State University of New Jersey

In partial fulfillment of the requirements

For the degree of

Doctor of Philosophy

Graduate Program in Pharmaceutical Science

Written under the direction of

Patrick J. Sinko

And approved by

_____

_____

_____

_____

New Brunswick, New Jersey

JANUARY, 2015

ABSTRACT OF THE DISSERTATION

Molecular-size Effects of Poly(ethylene glycol) Doxorubicin Nanocarriers on the Intraductal Treatment of Ductal Carcinoma in Situ (DCIS)

By ZICHAO GU

Dissertation Director:

Patrick J. Sinko

Systemic chemotherapy is not a first-line treatment option for early stage breast cancer due primarily to the limited blood supply in mammary ducts and the variable and limited drug concentration reaching to the tumor within the ducts. To enhance local drug concentration and avoid excess systemic exposure, an intraductal approach for delivering the anti-cancer agents directly to mammary glands provides an alternative method for treating DCIS.

Doxorubicin (DOX) is a widely used anti-cancer drug but it rapidly diffuses from the mammary gland into the systemic circulation. Therefore, techniques for retaining drugs locally in the mammary gland are needed. The objective of this thesis project is to design,

develop, and evaluate breast intraductal drug delivery systems that provide higher drug retention in the mammary gland, thereby minimizing systemic exposure and achieving maximal local therapeutic effect. PEG polymers with different molecular weights (5, 10, 20 and 40 kDa) and molecular architectures (linear, four-arm and eight-arm) were conjugated to DOX to develop PEG DOX (PEG-DOX) nanocarriers. The hydrodynamic radii studies showed the hydrodynamic radii increased with increasing molecular weight for the linear PEGs and decreased with increased branching in the polymer structure. The mammary gland retention half-lives demonstrated the influence of molecular weight and structure of nanocarriers on mammary gland retention. Pharmacokinetic profiles indicated that nanocarriers with longer retention half-life tend to distribute into the blood stream with a delayed plasma peak time. Histological studies showed no local damage or inflammation in the nanocarrier treated mammary gland, but altered ductal structure was observed in DOX treated mammary gland.

A F344 tumor model, developed by inoculating 13762 Mat B III cells into female F344 rats intraductally, exhibited cell load- and time-dependent tumor development in the rats. Efficacy studies demonstrated slower tumor growth in the intraductal treatment groups than in the intravenous treatment groups. The survival rate in the intraductal treatment groups was significant higher than the untreated group. In summary, the developed PEG-DOX nanocarriers improved DOX retention and reduced DOX toxicity in mammary gland, leading to a significantly improved survival percentage in treating DCIS in a F344 tumor rat model.

DEDICATION

To my parents, Jilin Gu and Ruirui Zhang,

Who always gave support and taught me the importance of independence and happiness.

To my supervisor, Professor Patrick J. Sinko,

Who has always given me valuable suggestions and generous encouragement.

Thank you for all your support.

ACKNOWLEDGEMENTS

First and foremost, I am very thankful for my loving family who supported and inspired me to make this dissertation possible. I am deeply indebted to my parents for their endless patience and support. Thanks to my dearest friend Vivien Pu for her encouragement that made me look at life in a more positive perspective.

I would like to express my gratitude to my supervisor, Dr. Patrick J. Sinko, who has supported me through all the time of research with his patience, guidance and advice. I attribute the level of my Ph.D. degree to his encouragement and effort and without him this thesis would not have been possible to be completed.

I would like to thank my committee members: Dr. Bozena Michniak-Kohn, Dr. Guofeng You and Dr. Susan Love for their helpful advice and time.

I am grateful to many of my former and present members in Dr. Sinko's group: Dayuan, Yash, Mary, Derek, Steven and Zoltan for their support and help on my research. I would also like to thank my other lab mates for their support and friendship, Hui Pung, Marianne Shen, Sharana Taylor and other colleagues in the Department of Pharmaceutics for their assistance and patience.

Lastly I offer my regards and blessings to all of those who supported me in any respect during the completion of my thesis.

TABLE OF CONTENTS

LIST OF TABLES

LIST OF FIGURES

1 INTRODUCTION

Ductal Carcinoma in Situ (DCIS) is an early stage breast cancer in which all of the malignant epithelial cells are confined within the breast ducts [1]. It is considered a major health concern because it is generally believed that it represents a stage in the progression to invasive breast cancer [2]. Systemic chemotherapy is not a first-line treatment option for DCIS mainly because there is a limited blood supply in mammary ducts. This inefficient tissue perfusion results in low and variable drug concentrations in the diseased ducts. Direct administration into the breast duct (i.e., an intraductal approach) may resolve the issue of achieving therapeutically effective local concentrations by delivering the drugs directly to mammary ducts. However, minimizing excessive systemic exposure due to rapid clearance from the duct remains a significant challenge.

Doxorubicin (DOX) is an anthracycline antibiotic used to treat various cancers. Generally it is believed to exert anti-tumor effects by specific intercalation and inhibition of macromolecular biosynthesis [3, 4]. However its applications are limited due to its toxic effects on various organs, which may be a result of non-specific intercalation and cell membrane binding. Administering DOX into the local diseased ducts may limit the toxicity to healthy tissues and organs arising from systemic treatment. Since DOX is a small molecule drug with a molecular weight of 543.52 g/mol, when administered intraductally, it may diffuse rapidly out of the duct resulting in a short local retention half-life. Therefore designing and developing a drug delivery system that improves retention of DOX in mammary duct, thereby limiting undesired side effects and providing more efficacious treatment for DCIS is urgently required.

PEGylation is a process of attaching proteins, peptides or small organic molecules to polyethylene glycol (PEG) polymers [5]. It can be used to modify small molecule anti-cancer drugs by overcoming obstacles such as low solubility, high toxicity, short elimination half-life or untargeted biodistribution [6]. Therefore, it is hypothesized that attaching DOX to PEG polymeric nanocarriers will prolong the retention time and reduce the toxicity of DOX in mammary ducts.

A breast cancer animal model with development of early stage lesions is important for preclinical studies of DCIS. The 1-Methyl-1-nitrosourea (MNU) model is a frequently used model developed by Thompson et al. [7]. Numerous premalignant and malignant lesions can be induced 35 days after i.p injection of MNU into female Sprague-Dawley rats. A significant limitation to the approach is that all 12 mammary glands need to be treated since the lesions may develop in any of the mammary glands. A subcutaneous model is another widely used model. However, the injected cells do not proliferate in the local mammary gland environment and lesion formation is low [8, 9]. A human-in-mice (HIM) model has a high rate (~90%) of formation of DCIS-like lesions by 6 weeks after cell injection [10], the experimental method applied is invasive and time-inefficient since the inguinal gland must be exposed to ease intraductal inoculation. So it is crucial to develop a new DCIS animal model, which initiates tumor growth in the ductal microenvironment.

This thesis aims to develop DOX PEG nanocarriers using PEG polymers of varying

molecular weights and structures and to investigate their retention in mammary ducts of rats. Also it aims to establish an orthotopic rat breast cancer model and evaluate the efficacy of intraductally delivered DOX PEG nanocarriers in this model.

2 BACKGROUND AND SIGNIFICANCE

2.1 Breast cancer

Breast cancer is the most common type of cancer among women in both developed and developing countries [11, 12]. It is the leading cause of cancer death in females worldwide, accounting for 23% of the total cancer cases, and 14% of the cancer deaths in 2008 [11]. In US, approximately 232,340 new cases of invasive breast cancer and 39,620 breast cancer deaths are expected to occur among women in 2013 [13]. Moreover, one in eight US women will be diagnosed with invasive breast cancer over the lifetime [13].

Breast cancer is a multifactorial disease, and it develops in women as the result of a combination of both endogenous and exogenous factors [14]. The risk of developing breast cancer is associated with various factors, including age, gender, family history, reproductive, environmental and endogenous factors [15-18]. The risk of the disease increases with increasing age. The annual incidence of breast cancer in the US women aged 80-85 is 15 times higher than that in women aged 30-35 [19]. Alcohol consumption also increases the risk of breast cancer. [20]. Furthermore, risk of developing breast cancer is largely linked to reproductive factors, including a long menstrual history, nulliparity, recent use of postmenopausal hormone therapy or oral contraceptives, and late age at first birth [21]. Specifically, risk of developing breast cancer is increased by early menarche, late menopause, and nulliparity, giving live birth for the first time after age 30. While the risk is reduced by higher parity and lactation [21]. Maintaining a healthy body weight, increasing physical activity, and minimizing alcohol intake are the best available strategies to reduce the risk of developing breast cancer [22].

Given its incidence and frequency, clinical researchers have focused on using effective methods to detect breast cancer at its earliest stages and standardized treatments to cure the disease early after its diagnosis. The axillary lymph node metastases and distant spread are present in about 40% and 5-15% of patients at the time of diagnosis respectively [23]. Moreover, even in patients at the early stage without metastases in axillary lymph node, recurrence can still be expected in up to 30%, which is probably due to circulating malignant cells [18]. These data emphasize that early diagnosis and prevention is the key to improve therapeutic effects, increase survival rates, and spare the patients from the invasive treatments or the potential adverse effects of toxic treatments, e.g. chemotherapy and/or radiation therapy [18]. Over the last 2-3 decades, breast cancer mortality rates have been steadily decreasing in the US [24], which is largely the result of early detection as well as improved targeted therapy [11, 24].

Usually at the early stage breast cancer, no symptoms may be felt. Therefore breast cancer screening is really pivotal in an attempt to achieve an earlier diagnosis. Monthly breast self-examination by the age of 20 years old is recommended [25]. In addition annual screening mammography beginning at age of 40 years old and clinical breast examinations every three years for women aged 20-40 years and yearly after age of 40 years old is recommended by the American Cancer Society [26].

The treatment plan includes surgery, radiation and systemic therapy (chemotherapy, hormonal therapy, or biologic therapy). And it depends on the size, stage, rate of growth

and other characteristics of the breast cancer [26]. Surgery will be performed as the first line treatment against early-stage breast cancer. While in patients with large tumor or bulky nodal disease, neoadjuvant chemotherapy will be applied to provide prognostic information. Radiation is given after surgery and chemotherapy to reduce the risk of breast cancer recurrence [26]. Further improvements in breast cancer treatment will continue to evolve.

2.2 Ductal Carcinoma in Situ (DCIS)

DCIS, defined as the proliferation of malignant cells without invasion of the basement membrane, is the most common type of non-invasive breast cancer [1, 2, 27-29]. The incidence had increased from 1.87 per 100, 000 women from 1973 to 1975 to 32.5 per 100,000 women in 2004 [30]. Furthermore it has been estimated that more than 1 million women will be diagnosed with DCIS by 2020 [30]. The dramatically increased incidence of DCIS can be explained by largely increased use of screening mammography [1, 31, 32]. Overall, the rate of increase in incidence of DCIS has been higher than any other type of breast cancer [1].

Since the majority of DCIS does not present with a palpable mass by physical examination, image-directed procedures are required for the diagnosis and treatment. DCIS is primarily diagnosed via mammography followed by stereotactic needle biopsy [33]. Mammography shows DCIS as a cluster of calcifications or microcalcifications, which appear either as white specks or as a shadow. In addition, new techniques such as

magnetic resonance imaging (MRI) and analysis of ductal cytology help to improve DCIS detection [33].

DCIS is thought to be part of a spectrum of proliferative lesions ranging from epithelial hyperplasia without atypia to microinvasive carcinoma [1]. Generally it is classified according to architectural pattern (papillary, micropapillary, cribriform, solid and comedo), nuclear grade (low, moderate and high grade), and necrosis (presence or absence) [1, 33]. However, groups categorized by architectural description do not take into account important prognostic features [1]. DCIS has been shown to be associated with an increased risk to develop invasive cancer based on laboratory and patient data though it is a benign lesion [33-35]. The lesions with higher nuclear grade and the presence of comedo narcosis are more likely to recur or progress to invasive breast cancer [36].

The main objective of treating DCIS is to prevent local recurrence, in particular of invasive breast cancer [2]. In the past, mastectomy was accepted as the primary treatment for patients with DCIS due to its extremely low risk of local recurrence (<1%), but now it should be reserved for patients with multicentric disease, large lesions, other contraindications to breast conservation, or a personal preference for mastectomy [1, 33]. Based on retrospective data, it shows that survival is similar among mastectomy, breast conservation with radiation, and breast conservation without radiation for the treatment of DCIS, and ranges between 98-100% [37, 38]. Now the more popular treatment option is lumpectomy (breast-conserving surgery) in which only the affected areas of breast are

excised. It is often followed with radiotherapy, which is used to reduce the risk of recurrence. There is general agreement that in most patients with non-multicentric DCIS, lumpectomy with postoperative breast radiation is as effective as a treatment as mastectomy with demonstrated decrease in local recurrence [35, 39, 40].

Since it is really hard to distinguish the location and extent of lesions that are more likely to progress to invasive breast cancer, all these DCIS lesions are usually treated with a combination of surgery, radiation and systemic therapies to prevent the risk of developing an invasive cancer [1, 30, 33, 37, 41]. However these therapies are associated with systemic side effects, reduced patients compliance and unnecessary expense of the heath care system.

In conclusion, an improved understanding of DCIS will help determine its clinical relevance to patients and will help develop effective treatment strategies. More research need to be done to prevent the consequent morbidity, mortality associated with invasive breast cancer.

2.3 Intraductal approach to treat breast cancer

2.3.1 Anatomy of the breast

Knowledge of human breast anatomy has important implications for understanding normal breast growth and development, the growth of carcinoma in situ along breast ducts, and feasibility of applying intraductal approach for diagnosis or treatment through duct opening on the nipple [42].

Human breast is a glandular organ with lobar morphology [43]. A typical breast lobe is a unit consisting of one lactiferous duct opening on the surface of the nipple, branching into segmental, subsegmental and terminal ducts that end as thousands of lobules [44, 45]. The terminal duct and the corresponding lobule, called as terminal ductal-lobular unit (TDLU), is the basic functional and histopathological unit in the breast [46].

Lobe is a complex dynamically evolving and involuting structure during the woman's entire lifetime [23]. Before puberty, there are relatively few TDLU [47]. The number of TDLU is the highest during the period of late pregnancy and lactation, and is substantially decreased after the menopause. Therefore the number of TDLU depends on women's age, constitution and hormonal status. On contrast, the number of the lactiferous ducts and the openings is constant during women's lifetime, independent of hormonal influences and age [23].

To define the number and arrangement of these lactiferous ducts, a considerable number of studies using histological, ductal, and imaging approaches have been conducted. The best study dates back to 1840 when Cooper injected colored wax into the ducts of over 200 breasts of women who died during lactation to study the breast duct anatomy (Figure 2.1) [43]. He stated the greatest number of lactiferous ducts that he was able to inject was 12 and more commonly 7-10 per nipple [43]. Teboul and Halliwell reported 5-8 'milk pores' in the nipple on more than 6000 ultrasound studies of the breast ducts [48]. Moffat and Going traced 10 complete non-anastomosing ductal systems by three-dimensional

computer model of a single autopsy breast [49]. Love and Barsky found an average of 5-9 ductal orifices over 200 lactating women [50]. Ramsay and colleagues described 6-12 main ducts by studied 21 lactating women with ultrasound [51]. In spite of this controversy about the exact number, they demonstrated that they were able to fill all of the ducts in mastectomy specimens by cannulating and instilling dye. And now it is generally accepted that the ductal system is a non-anastomosing system comprised of central ducts leading back to the chest wall and peripheral ducts draping over the central ducts [27, 42, 50], though rare anastomoses between the ductal systems have been described in one study [52].

In all, all these data suggest that there are 5 to 12 significant, non-anastomosing lactiferous ductal systems, which can be approached from the openings on the nipple [53].

Figure 2.1. Cooper's map of lactating ducts [43].

2.3.2 Intraductal Therapy

DCIS is thought to be part of a spectrum of proliferative lesions ranging from epithelial hyperplasia without atypia to microinvasive carcinoma [1]. Although it is non-invasive, DCIS has been shown to have the potential to evolve into invasive cancer [2, 35]. Therefore intervention at this stage is expected to prevent the occurrence of invasive breast cancer and provide significant health benefits to women. The main objective of treating DCIS is to prevent local recurrence, especially invasive breast cancer [2]. Treatment for DCIS ranges from lumpectomy to mastectomy, with or without radiation therapy [1, 2, 30, 33].

Chemotherapy is not used to treat DCIS since chemotherapeutics are administered predominately orally or intravenously. Though systemic route is the most efficient approach to deliver the agents to many organs or tissues, it also exposes the healthy organs or tissues to the delivered agents, resulting in undesired toxic side effects, such as hair loss, pain, and nausea. Systemic chemotherapy will make low and variable drug access to the mammary ducts due to the limited blood supply within the breast ducts. Intervention that is minimally invasive with lower systemic toxicity would be desirable for women having these noninvasive lesions or for those at higher risk. Since most breast cancers arise from ductal epithelial cells [2, 28, 29] and are located in a single lobe of one breast [44, 45, 52, 54]. The intraductal approach to deliver chemotherapeutics is particularly appealing in the local treatment for DCIS by targeting the carcinoma-containing lobe.

Several studies have been conducted successfully by using this local ductal delivery of various anti-cancer drugs. In 2003, McFarlin and Gould, for the first time, used the intraductal route to infuse retroviral vectors in mammary glands of rats to study the role of activated Raf in mammary carcinogenesis [55]. Okugawa et al. applied the concept of intraductal therapy in MNU-induced rat model, and reported significantly reduced tumor burden and total number of mammary carcinoma in the intraductally-administered paclitaxel group than in the intraperitoneally-administered paclitaxel group [56]. Moreover, they showed no toxic side effects were produced in the intraductally-administered paclitaxel group [56]. Murata et al. intraductally administered 4-hydroxy tamoxifen and PEGylated liposomal doxorubicin (PLD) in MNU-induced rat and HER-2/neu transgenic mouse model of breast cancer, and they observed more effective regression of tumor and lower systemic levels of PLD from the intraductal administration group than intravenous administration group [57]. Furthermore, a number of clinical trials have been conducted to explore the possibility of intraductal therapy in humans having DCIS or early stage invasive cancer. Mahoney et al. demonstrated the feasibility of intraductal therapy in treating women diagnosed with DCIS in a community setting [58]. Chen et al. investigated the difference in plasma concentrations of doxorubicin in female breast cancer patients treated with PLD by intraductal and intravenous route respectively [59]. Love et al. [60] investigated and demonstrated the safety of intraductally-administered PLD and carboplatin in women prior to mastectomy in a phase I clinical trial. It is interesting to note that ductal permeability of carboplatin appeared to be high in women suggesting that developing ductal retention strategies for small molecule drug is warranted. These studies suggest that the intraductal approach has

potential for applying prevention and neoadjuvant therapy of early breast cancer by providing higher local drug concentration with minimized systemic exposure.

Based on an emerging understanding of the anatomy of the breast and the novel techniques to access the ductal system, administration of agents directly into the breast ductal system through the nipple will provide an alternative way to prevent the progression of benign lesions or the development of new tumors.

2.4 Doxorubicin

Doxorubicin (DOX) is a widely used chemotherapy drug in the treatment of various cancers, most particularly breast cancer, childhood solid tumors, soft tissue sarcomas, and aggressive lymphomas [61]. It is a cytotoxic anthracycline antibiotic, which was isolated from cultures of *Streptomyces peucetius* early in the 1960s. It is amphoteric, containing acidic functions in the phenolic ring groups and a basic function in the sugar amino group [4]. The chemical formula of DOX is $C_{27}H_{29}NO_{11}$ with the molecular weight of 543.52 g/mol. The structure is shown as follows:

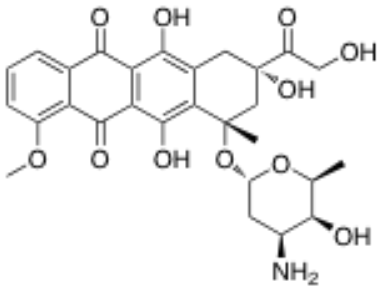

The recommended dosage for DOX to treat advanced breast cancer is 60 to 75 mg/m^2 every 21 days by intravenous route, in the form of hydrochloride salt. The brand names include Adriamycin PFS, Adriamycin RDF and Rubex [3, 62].

The mechanism of action of DOX against cancer cells is still somewhat unclear. Generally it is thought to interact with DNA by specific intercalation to inhibit the macromolecular biosynthesis [3, 4]. The planar ring of DOX intercalates between two base pairs of the DNA, while the external moieties (i.e., the daunosamine sugar and the cyclohexane ring) also seem to play an important role in the formation and stabilization of the ternary complex [61, 63, 64]. It also stabilizes the topoisomerase II complex in which DNA breaks are covalently linked to tyrosine residues of TOP II, preventing the DNA double helix from being resealed and thereby stopping the replication process, which is believed to be a persuasive mechanism of its antitumor activity [61]. Moreover, free radicals generated from the redox cycling activity of DOX damage macromolecules such as DNA and cell membranes [65]. One-electron addition to the quinone moiety results in formation of a semiquinone and the semiquinone quickly regenerates its parent quinone by reducing oxygen to reactive oxygen species (ROS) [61]. However the life-threatening cardiotoxicity of DOX is believed to be associated with the formation of ROS, which causes damage to cardiomyocytes, leading to myofibrillar loss and cytoplasmic vacuolization [61].

As an anticancer drug, DOX shows high cytotoxicity in malignant cells, however, it causes acute adverse effects, including nausea, vomiting, heart arrhythmias, neutropenia

and complete alopecia. When its cumulative dose reaches more than 500 mg/m^2, the risks of developing cardiac toxicity increase significantly [66]. Because of its serious adverse effects and its red color, DOX has an informal term as “the red devil” or “the red death”. Thus, a local delivery system designed with reduced systemic toxicity becomes necessary to lower the toxicity to normal tissues and deliver the drug directly to the cancer cells.

2.5 PEGylation in Drug Delivery

PEG is a synthetic polymer comprised of repeating ethylene oxide subunits with molecular weight of 44 Da [67]. It is water-soluble, amphiphilic, nontoxic, non-immunogenic and safely eliminated by a combination of renal and hepatic pathways [67, 68]. And it has been approved by FDA for human oral, intravenous, and dermal pharmaceutical applications [68]. Due to these favorable properties, PEG plays an important role in drug delivery.

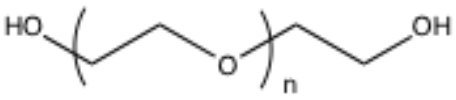

Poly(ethylene glycol) (PEG)

In the 1970s, the technique of PEGylation was first published by Abuchowsky et al., for the modification of albumin and catalase [69, 70]. Generally it is described as a process of covalently attaching proteins, peptides, or small organic molecules to polyethylene glycol (PEG) polymers [5]. The primary usage of PEGylation was in proteins, peptides,

and oligonucleotides. The advantages of using PEG for these macromolecular drugs delivery are increased solubility and stability, prolonged plasma half-life, reduced immunogenicity, decreased degradation by metabolic enzymes, and lower renal clearance and uptake by the cells of reticuloendothelial system (RES) [69-74].

To date, ten PEGylated proteins, antibody fragments, and oligonucleotides have been approved by FDA [75]. For example, PEG conjugates of enzymes like adenosine deaminase (Adagen®) [76] and L-asparginase (Oncaspar®) [77] received FDA approval in 1990 and 1994 for the treatment of severe combined immunodeficiency syndrome and acute lymphoblastic leukemia (ALL). Later, two PEG conjugates of biological response modifier interferon-α (IFNα), PEGylated interferon α-2a (Pegasys®) [78-80] and PEGylated interferon α-2b (PegIntron®) [79, 80] were approved for the treatment of diseases such as hepatitis C infection and chronic myelogenous leukemia. In 2010, the PEGylated porcine-like uricase (Krystexxa®, Puricase®) was approved for the treatment of severe, treatment refractory chronic gout [81].

The successful clinical application of PEGylated biomacromolecular drugs has promoted the usage of this technique in small molecular drugs to overcome the shortcomings associated with the therapy. Small molecular drugs, especially the anti-cancer agents, often have some problems, such as low solubility, high toxicity, short elimination half-lives or non-targeted biodistribution [6]. To overcome the obstacles, one promising approach is to use PEGylation strategy. Compared to biological macromolecules, small organic molecules present fewer problems in the technique of PEGylation since they have

fewer functional groups, lower conformational constraints, and easier purification and characterization steps [82]. In all cases, the attachment of PEG to drugs can significantly prolong the circulation time of the drugs since the PEGylated conjugates barely permeate through the endothelium of normal blood vessels.

2.6 Animal models of Breast cancer

Most breast cancers begin in the tissues of the breast, usually developing from the inner lining of milk ducts which drain milk from the lobules to the nipple, or the lobules which produce milk [83]. It is the most common type of cancer among women worldwide [11, 12]. Over the course of a life-time, 1 in 8 U.S. women will be diagnosed with invasive breast cancer [13].

Since more and more potential therapeutic strategies become available to improve survival rates of patients with early stage breast cancer, development of in vivo breast cancer animal models is crucial to help with the preclinical trials. Several animal models have been established and characterized for the preclinical studies. 1-Methyl-1-nitrosourea (MNU) model is a carcinogen induced breast cancer model established by Thompson et al. [7]. This model is developed by using i.p. injection of MNU into female Spargue-Dawley (SD) rats at 20 days of age [7]. It provides rapid induction of premalignant and malignant stages of mammary carcinogenesis. A numerous premalignant and malignant lesions can be rapidly induced 35 days postcarcinogen injection [5]. Intraductal injection is feasible in all 12 mammary glands. However, the tumor may grow in any of the 12 mammary glands and thus requires treatment of all 12

mammary glands. Subcutaneous model is another frequently used model. It is very convenient, but a potential disadvantage is that the cancer cells are not orthotopically inoculated in mammary ductal environment, leading to a low take rate [8, 9]. And the model may lack the consistent invasive and metastatic behavior. To overcome these disadvantages, there have been several efforts to develop orthotopic models for breast cancer by inducing the tumors in organ of origin in the rodents. It can significantly increase the take up rate of tumors and occasionally facilitate metastatic spread that will not occur in subcutaneous model [84, 85]. The intraductal human-in-mouse transplantation model established by Behbod et al. [10] shows a high take up rate at 90% and DCIS-like lesions by 6 weeks after injection. However in their experimental procedures, they make a Y-incision to expose the inguinal gland for the ease of injections and inject cells via cleaved nipple. Though this orthotopic model initiates tumor growth in local ductal environment, the intraductal inoculation is really invasive and time-consuming.

Therefore, it is necessary to generate new animal models that more accurately recapitulate breast cancer progression, while offering the advantages of model systems, such as tumor initiation in ductal microenvironment, easy operation and pharmacological manipulation.

3 SPECIFIC AIMS

Ductal carcinoma in situ (DCIS) is a noninvasive stage 0 breast cancer in which the cancer cells are still confined within a mammary duct. It is considered a major health concern because, if untreated, it may progress to invasive breast cancer. Systemic chemotherapy is generally not used to treat DCIS because mammary ducts have limited blood supply and the location of cancer within the ducts makes access to the drug variable and unreliable. In addition, systemic administration will expose patients to undesirable drug toxicities. Since the DCIS is confined within the mammary ducts, delivering anti-cancer agents directly to the affected duct (intraductal) could be a more effective treatment method. The benefits of using an intraductal approach are local targeting combined with low systemic exposure. However, because most drugs used in chemotherapy are small molecules, they will rapidly diffuse out of the mammary duct. Therefore, there is an urgent need to design, develop, and evaluate intraductal drug delivery systems that provide higher retention in the mammary gland, thereby optimizing treatment efficacy while minimizing systemic exposure and undesired side effects.

This thesis aims to design, fabricate, and evaluate polymeric nanocarriers for intraductal delivery of doxorubicin (DOX) for treating DCIS while minimizing side effects. It aims to investigate the retention of DOX in mammary ducts after PEGylation. It also aims to establish an orthotopic rat breast cancer model and evaluate the efficacy of intraductally delivered nanocarriers in treating DCIS in an animal model. The drug delivery systems prepared in this work are expected to improve drug retention in ducts (local targeting), leading to improved tumor regression and are also expected to significantly reduce

systemic exposure to chemotherapy.

The specific aims of the proposed thesis project are as follows:

Specific Aim 1: to develop PEG DOX nanocarriers using PEG polymers of different molecular weight and structure, and to investigate their ductal retention.

Hypothesis

PEGylation of DOX will improve its retention in the mammary duct due to the increase in effective molecular size of DOX.

Rationale

Most therapeutic agents are small molecules and are expected to rapidly diffuse out of the ducts. In our previous study, fluorescein, a diagnostic moiety, was conjugated to PEG polymers of varying molecular size. After intraductal administration into SD rats, the ductal retention of fluorescein showed molecular size-dependency. We are using these results and approach to improve the ductal retention of intraductally delivered DOX, which is also a small molecule (MW: 540 Da). Conjugating DOX to PEG nanocarriers will increase its effective molecular size and hence the ductal retention.

Specific Aim 2: to establish an orthotopic rat breast cancer model to mimic human breast cancer progression in a mammary ductal environment.

Hypothesis

If cancer cells are inoculated directly into the mammary duct, tumors will originate from the orthotopical site. Therefore, the developed model will more closely mimic the human breast cancer progression than other currently used models.

Rationale

Various animal breast cancer models have been established and utilized in preclinical studies, but none of them mimic the anatomic onset. For example, the MNU-model is a carcinogen induced breast cancer model. Tumors may develop in all twelve mammary ducts of rats over the time. In this case, the treatment of early lesions requires administration of therapeutic agents to all of the twelve mammary ducts. Likewise, subcutaneous models are very convenient and frequently used, but tumors are not induced in the mammary duct environment. Intraductal inoculation of cancer cells will help to initiate tumor growth and mimic human breast cancer progression in the ductal microenvironment.

Specific Aim 3: to evaluate the feasibility of delivering PEG nanocarriers intraductally for treating DCIS in a F344 tumor model.

Hypothesis

Intraductal therapy will treat mammary tumors developed in the F344 breast cancer model more effectively than with intravenous administration due to enhanced local drug concentration in the mammary ducts.

Rationale

Systemic chemotherapy is not widely used to treat DCIS due to the limited blood flow to the mammary ducts; an intraductal approach provides an alternative treatment option for early stage breast cancer. Since the drugs are directly administered to the diseased duct, intraductal therapy will offer higher local drug concentration and limited systemic toxicity, leading to improved efficacy with respect to systemic route.

4 DESIGN AND INVESTIGATE THE KINETICS OF DOX CONTAINING PEG NANOCARRIERS WITH VARYING MOLECULAR WEIGHTS AND STRUCTURES IN RAT MAMMARY GLAND

4.1 Introduction

Doxorubicin (DOX), a cytotoxic anthracycline antibiotic, is one of the most effective anticancer drugs in the treatment of various cancers, most particularly breast cancer, childhood solid tumors, soft tissue sarcomas, and aggressive lymphomas [61, 86]. The detailed mechanism of drug action is still somewhat unclear. However, a persuasive mechanism is that it exerts anticancer effects by stabilizing the topoisomerase II complex after it breaks the DNA chain, preventing the DNA double helix from being resealed and thereby stopping the replication process [61]. And it also intercalates between DNA base pairs to prevent the macromolecular biosynthesis [3, 4]. In addition, reactive oxygen species (ROS) damage is believed to be another mechanism too [61]. Although DOX shows high cytotoxicity against malignant cells, its clinical utility is limited by dose-dependent toxicity (myelosuppression and cardiotoxicity) [87]. In early stage breast cancer treatment, chemotherapy is not a first option because of the undesired side effects arising from systemic administration. To avoid the excess systemic exposures, delivering DOX directly into mammary ducts provides an alternative approach to achieve the treatment goal. However, when we administered DOX directly into the mammary duct, it diffused out of mammary gland fast with short mammary gland retention half-live of

1.97±0.35 hr. Therefore a drug delivery system is required to improve the retention and reduce toxicity of DOX in mammary ducts.

PEGylation is a process in which poly(ethylene glycol) (PEG) is covalently attached to the therapeutic agents [69, 88]. It was firstly described in 1977 by modifying bovine serum albumin [69] and bovine liver catalase [88]. PEG polymer has been approved by FDA for human oral, intravenous and dermal pharmaceutical applications due to its non-toxicity, non-immunogenicity, non-antigenicity and amphiphilicity [68]. Along with reduced immunogenicity and antigenicity, conjugating DOX to PEG helps to increase water solubility, prolong plasma half-life, and reduce toxicity [6, 74].

Herein, the current studies aimed to investigate the ductal retention and toxicity of DOX after PEGylation. PEGs of varying molecular weights (5, 10, 20, 40 kDa) and structural configurations (linear, four-arm and eight-arm) were used as nanocarriers and DOX was conjugated to the PEGs. The mammary gland retention of PEG nanocarriers in Sprague Dawley (SD) rats and toxicity in MCF-7 cell line (a breast cancer cell line) and in local mammary glands of SD rats were evaluated. Systemic pharmacokinetics of nanocarriers upon intraductal administration were also investigated.

4.2 Materials and methods

4.2.1 Materials and instruments

Doxorubicin hydrochloride was obtained from Changsha Huajia Chemicals (Hunan, China). N, N-Dimethyl formamide (DMF) Diisopropylethyl amine was obtained from Sigma-Aldrich (St. Louis, MO), whereas Sephadex G50 and G25 (medium) were obtained from Thermo Fisher Scientific (Suwanee, GA). All cell culture reagents were obtained from Invitrogen (Carlsbad, CA), and Aerrane (isoflurane) was obtained from Baxter Healthcare Corporation (Deerfield, IL). The nanocarriers (2 mg/mL) were analyzed using High Performance Liquid Chromatography (HPLC) equipped with ultraviolet (UV) and fluorescence detectors; Stability studies were carried using a Symmetry 300^{TM} C18 column (5.0 μm, 4.6 mm × 50 mm column) (Waters, Milford, MA). The hydrodynamic radii of polymers were measured by dynamic light scattering (DLS) on a Malvern Zetasizer Nano ZS. The animal body images were obtained non-invasively on a Xenogen IVIS® 100 imaging system from Caliper Life Sciences (Hopkinton, MA). The plasma samples were analyzed by using a guard column combined with Waters Symmetry C18 column (5.0 μm, 4.6 mm × 250 mm column).

4.2.2 Synthesis and characterization of PEG DOX (PEG-DOX) nanocarriers

PEG-NHS (linear 5, 10, 20, 40 kDa, four-arm 40 kDa and eight-arm 40 kDa) polymer (200 mg) was dissolved in 10 mL DMF containing 20 μL DIEA, and doxorubicin hydrochloride (2.5 equivalent for each functional group of PEG) was added to the polymer solution. The reaction mixture was left stirred in dark at room temperature for 8

hours. All nanocarrier reaction mixtures were purified on a Sephadex G25 (5 kDa) or G50 (10-40 kDa) column using deionized water as eluent. The high molecular weight fraction was collected and lyophilized to obtain pure nanocarriers and characterized using HPLC with UV and fluorescence detection.

4.2.3 Hydrodynamic radii measurements

The hydrodynamic radii of PEG-DOX nanocarriers were tested at room temperature using DLS. The nanocarriers (2 mg) were dissolved into deionized water (1 mL) and passed through a 0.2-μm membrane filter prior to each measurement. All studies were performed in quintuplicate and data are presented as mean ± SD.

4.2.4 Stability studies

The PEG-DOX nanocarriers (2 mg) were dissolved in 0.1 M sodium phosphate buffer (pH 7.4, 1 mL). The glass vials containing the nanocarrier solution were placed in an incubator (37 ℃) during for three weeks. Aliquots (20 μL) were pulled from the vials at predetermined time points and were evaluated by using HPLC equipped with fluorescence detector (excitation wavelength: 480 nm, emission wavelength: 590 nm). Water containing 0.1 % trifluoroacetic acid (TFA) (solvent A) and 100% acetonitrile containing 0.1% TFA (solvent B) was used as the mobile phase. The gradient was run from 5-100% of solvent B in 6 min.

4.2.5 *In vitro* studies

4.2.5.1 Cell culture

The MCF-7 cell line, which is a human breast cancer cell line, was obtained from American Type Culture Collection (Manassas, VA) and was maintained in DMEM (Invitrogen, Carlsbad, CA) supplemented with 10% fetal bovine serum (FBS) (Fisher Scientific, Fairlawn, NJ), 1% penicillin/streptomycin and 0.01 mg/mL insulin at 37 ℃ in a humidified atmosphere of 5% CO_2 (v/v) in air.

4.2.5.2 *In vitro* cytotoxicity studies

The cytotoxicity studies were assessed by (3-(4,5-Dimethylthiazol-2-yl)-2,5-diphenyltetrazolium bromide (MTT) assay. MCF-7 cells were seeded in 96-well plate at 4000 cells per well and incubated for 24 hours. At 24 hours, PEG-DOX nanocarriers were added and incubated for 48 hours. At 48 hours, 100 μL of MTT solution was added into each well. The medium was removed after 2 hours, and 100 μL of DMSO was added into each well to dissolve the crystals by mixing on a shaker for 5 min. The UV absorbance was determined using plate reader at 570 nm.

4.2.6 *In vivo* studies

4.2.6.1 Animals

Sprague-Dawley (SD) female rats (6-8 weeks of age, weighing 182-209 g) were obtained from Hilltop Lab Animals, Inc. (Scottdale, PA), and housed in Rutgers Laboratory

Animal Services facility. The animals were maintained on a 12-h light/dark cycle in a temperature-controlled environment, with food and water *ad ilbitum*. The animals were acclimatized for at least a week prior to studies, and all procedures were performed according to the guidelines set by the National Institute of Health Guide and protocol approved by the Rutgers University Institutional Animal Care and Use Committee. One day prior to the mammary gland retention studies, the rats were put under anesthesia with isoflurane. The abdominal hair was trimmed with a clipper and skin hair was removed using Veet.

4.2.6.2 Mammary gland retention studies in female SD rats

The female SD rats (3 rats per group) were anesthetized with isoflurane and placed under a surgical microscope. The number four nipple on the left side was cleaned with 70% ethanol or isopropanol. After dilation of the orifice, the nanocarrier solutions or DOX (0.83 mg/kg/duct DOX equivalent in 100 μL DI water) were administered intraductally into the teat using a 33 G blunt-ended needle attached to a Hamilton syringe (Hamilton, Reno, NV). DOX was used as control. Rat body images were taken on an IVIS® 100 optical imaging system at various time points. The following instrument settings were used: Level: High; Em: DsRed; Ex: GFP; Bin: hr (4), FOV25, Aperture: f4, and shutter: 1s. Fluorescent intensity of area injected with nanocarriers or DOX was obtained by subtracting the uninjected area prior to analysis. Images were acquired and analyzed using Living Image 2.5 software (Caliper Life Sciences, Hopkinton, MA). Fluorescence intensities were plotted against time and retention $t_{1/2}$ in rat mammary gland was estimated by non-compartmental pharmacokinetic model using PKSolver [4]. The

numbers of points for the terminal slope were set to auto (default). Each data point represents mean ± SD (n=3).

4.2.6.3 Pharmacokinetic studies

The nanocarrier solutions and DOX were injected to the duct of mammary gland of female SD rats at a dose of 0.83 mg/kg/duct DOX equivalent. Blood samples were collected from tail vein into the heparin-treated microtubes at given time points (as indicated in the plots). Plasma was isolated immediately from the whole blood by micro-centrifugation (2000 g for 5 min) and was stored at -80 ℃. Prior to analysis, the plasma samples were thawed and processed using acetonitrile (4 times volume) to precipitate the proteins. The obtained supernatant was analyzed by RP HPLC equipped with fluorescence detector (excitation wavelength: 480 nm, emission wavelength: 590 nm). Water containing 0.1 % trifluoroacetic acid (TFA) (solvent A) and 100% acetonitrile containing 0.1% TFA (solvent B) was used as mobile phase. The gradient was run from 25-80% of solvent B within 20 min. The results were normalized using nanocarrier standard curves in plasma. The maximum concentration (c_{max}), the corresponding sampling time (t_{max}) and elimination $t_{1/2}$ were estimated by non-compartmental analysis using PKSolver [4]. The numbers of point for terminal slope were set to auto (default). Each data point represents mean ± SD (n=3).

4.2.7 Histological studies

Three animals were euthanized by CO_2 asphyxiation at 6 days post intraductal administration of nanocarriers and DOX. The mammary glands were excised and fixed in 10% neutral formalin solution for 24 hours before being further processed. Sections of the mammary glands were dissected and dehydrated through a series of graded ethanol baths and then infiltrated with paraffin. The infiltrated specimens were then embedded into paraffin blocks, which were sectioned to 5-micron thickness and mounted onto glass slides. The tissue slides were stained using hematoxylin and eosin (H&E) performed by Goody Histolab (New Brunswick, NJ) and observed histopathologically under a microscope to check for any possible ductal structure change caused by the administration of DOX or nanocarriers.

4.2.8 Statistical analysis

Experimental values were expressed as mean ± SD. Significance level was set as $p<0.05$. Parameters of mammary gland retention and plasma pharmacokinetics were estimated with PKSolver [4].

4.3 Results and discussion

4.3.1 Synthesis and characterization of PEG-DOX nanocarriers

PEG-DOX nanocarriers, in the molecular weight range 5-40 kDa, were prepared by coupling the DOX to PEG-succinimidyl ester. The PEG-succinimidyl ester (5 kDa, 10 kDa, 20 kDa, 40kDa, four-arm 40 kDa, eight-arm 40 kDa) as shown in Figure 4.1, was

reacted with the amine group of DOX at room temperature in DMF/DIEA for 6 hours (Scheme 4.1). All reactions were carried out in the dark and the reaction mixtures were purified on Sephadex column (G50 and G25 for 5 kDa) using water as eluent. The nanocarrier yields were in the range of 69-89%, suggesting a highly efficient coupling, except the yield of 40 kDa PEG-$(DOX)_8$ was 20%.

The purity was determined by HPLC equipped with UV and fluorescence detector. The retention time for the corresponding PEG-DOX nanocarriers (5 kDa, 10 kDa, 20 kDa, 40 kDa, four-arm 40 kDa, eight-arm 40 kDa) were 4.276, 4.190, 4.148, 4.128, 4.198, and 4.276 min, respectively. The retention time of the unreacted DOX was around 3.745 min. All nanocarriers were obtained in high purity (≥98%) (Table 4.1). Since the PEG polymer is more hydrophilic compared to the prepared nanocarriers, the PEG was not detected in the chromatogram. However, upon conjugation with DOX, all nanocarriers showed peaks in the UV channel as in the fluorescence channel, indicating the covalent attachment of DOX to the PEGs. The drug loading efficiencies were determined within the range of 1.03-4.46 wt.% (Table 4.2) by using a fluorescence spectrophotometer.

DLS was used to evaluate the influence of polymer molecular weight and structure on the hydrodynamic radii of unmodified PEGs. In Table 4.3, as the molecular weight increased from 5 to 40 kDa, the hydrodynamic radii increased from 2.661 ± 0.161 to 7.375 ± 0.454 nm. At the same molecular weight (40 kDa), when the polymer structure was changed from linear to branched (four-arm, eight-arm), the hydrodynamic radii decreased from 7.375 ± 0.454 to 5.622 ± 0.389 nm. The hydrodynamic radii of 5, 10, 20, 40 kDa, four-arm

40 kDa and eight-arm 40 kDa polymers were estimated as 2.661±0.161, 2.699±0.709, 4.521± 0.681, 7.375± 0.454 nm, 6.199±0.403, 5.622±0.389 nm, respectively. The hydrodynamic radii increased with an increase in molecular weight for the linear. But for the same molecular weight, the hydrodynamic radii decreased with increase in branching in the nanocarrier polymer structure. As described earlier, molecular size of polymers is influenced by molecular weight, chemical nature, shape and conformation in water.

The amide bond stability of nanocarriers was determined by incubating nanocarriers in 0.1 M sodium phosphate buffer (pH= 7.4) at 37℃ for 20 days (Figure 4.2). A quick degradation was observed in the first week, which might be related to the solution system. And the degradation slowed down afterwards, which can be explained by reaching equilibrium between prodrug and degradation products of prodrug after initial quick degradation within a few days.

4.3.2 *In vitro* cytotoxicity studies

The *in vitro* cytotoxicity studies were performed against MCF-7 cells by using MTT assay. The data were fit to a sigmoidal nonlinear regression model, and the concentration at which 50% of the cells were viable (IC50) was calculated on the basis of the best-fit model. As shown in Table 4.4, the IC50 value of DOX administered to MCF-7 cells was estimated to be 0.14 μM. The IC 50 values of linear 5 kDa, 10 kDa, 20 kDa, 40 kDa, four-arm 40 kDa and eight-arm 40 kDa PEG DOX nanocarriers were 1.76, 3.86, 8.96, 18.11, 1.23 and 3.49μM separately. All were about at least 8.8-fold less potent than their parent drug, free DOX.

4.3.3 Mammary gland retention studies in female SD rats

The mammary gland retention of nanocarriers was measured using an IVIS® 100 small animal imaging system. The nanocarriers (0.83 mg/kg/duct) and DOX were administered intraductally through the left number four teat in normal SD rats, which were anesthetized at different time points to obtain whole body images. Three female SD rats were used per group. In Figure 4.3, DOX exhibited extremely short retention in the mammary gland, with signals diminishing within 4 hours. On the other hand, the PEG-DOX nanocarriers showed prolonged retention in the mammary gland. Fluorescence signals were observed for up to 7 hours for the 5 kDa and 20 kDa, and 12 hours for the linear and branched 40 kDa nanocarriers. Thus, an increase in molecular weight led to longer retention in mammary ducts presumably, due in part, to hindered diffusion.

Fluorescence intensities from the injected area were plotted against time (Figure 4.4). The mammary gland retention half-life, $t_{1/2}$, defined as the time required for fluorescence intensity to reach 50% of its peak value, was estimated from plots by non-compartmental analysis using PKSolver. In Table 4.5, the $t_{1/2}$ of DOX was estimated as 1.97 ± 0.35 h, whereas the $t_{1/2}$ of linear 5 kDa and 20 kDa was 2.23 ± 0.28 h, and 3.59 ± 0.61 h, which increased to 13.11 ± 3.41 h for 40 kDa PEG-DOX. In Figure 4.5, $R^2 = 0.7308$, indicating a correlation between the mammary gland retention half-life and molecular weight of nanocarriers. For nanocarriers at the molecular weight of 40 kDa, the $t_{1/2}$ of eight-arm nanocarrier (11.90 ± 2.91 h) were lower than corresponding linear nanocarrier (13.11 ± 3.41), possibly due to more compact nature of the branched nanocarriers. The $t_{1/2}$

of four-arm 40 kDa (19.24±6.15 h) was longer than linear 40 kDa nanocarrier, which might be a result of variability in animal studies. In summary, the results obtained correlated well with the hydrodynamic radii reported in Table 4.3 suggesting that both the polymer molecular weight and structure influences the retention in the mammary gland.

4.3.4 Pharmacokinetic studies

Linear 5 kDa, 40 kDa, four-arm 40 kDa, eight-arm 40 kDa nanocarriers and DOX were administered to SD rats to assess the pharmacokinetics (t_{max}, c_{max} and plasma $t_{1/2}$). The plasma concentration-time data are shown in Figure 4.6. t_{max}, c_{max} values are reported in Table 4.6. The c_{max} for 5 kDa PEG-DOX, 40 kDa PEG-DOX, 40 kDa PEG-$(DOX)_4$ and 40 kDa PEG-$(DOX)_8$ were 1.67±0.58 h, 32± 6.93 h, 9.33± 2.31 h respectively, but the c_{max} for DOX was reached in only 0.23±0.23 h only. Thus, t_{max} increased in the order: free DOX < 5 kDa PEG-DOX< 40 kDa PEG-$(DOX)_8$ < 40 kDa PEG-$(DOX)_4$, similar to their order of retention in mammary gland. Moreover the c_{max} of linear and branched 40 kDa nanocarriers were higher than DOX and 5 kDa PEG-DOX because DOX and 5 kDa PEG-DOX were eliminated from the plasma with a t1/2 of 1.70±1.28 h, 11.39±5.25 h, but 40 kDa PEG-$(DOX)_4$ and 40 kDa PEG-$(DOX)_8$ stayed longer with a t1/2 of 104.00±41.08h, 56.49 ±28.65 h. This is due to the fact that molecular weight of 40 kDa nanocarriers are close to the renal threshold which for globular protein is ~ 40-60 kDa, and therefore they tend to remain in the blood circulation for longer durations.

4.3.5 Histological studies

SD rats treated with PEG-DOX nanocarriers and DOX (0.83 mg/kg/duct DOX equivalent) were euthanized 6 days after treatment. In Figure 4.7, the histological diagnosis of mammary ducts revealed that DOX damaged the mammary ducts and cause inflammation, which can be found from increased inflammatory cells surrounding ducts and among fat tissues. In the mammary ducts treated with nanocarriers, no inflammation was observed, but damaged epithelial cells in epithelium layer and detached cell debris were found in all treatment groups. Since most breast cancer cells arise from the epithelial cells, if the epithelial layer can be stripped, the abnormal or cancerous cells can be killed to achieve a therapeutic effect. Moreover, application of PEG-DOX nanocarriers helps to reduce the inflammation caused by DOX.

4.4 Discussion

Intraductal therapy has been introduced to treat DCIS in recent years [89, 90]. This therapy is designed to deliver therapeutic agents directly to the diseased breast duct. Upon intraductal administration, most drugs show a delayed t_{max} in the systemic circulation and a substantially lower systemic exposure than after intravenous administration suggesting slow absorption and reduced permeability from the duct. Murata *et al*. [91] evaluated the efficacy of PEGylated liposomal doxorubicin (PLD) in N-methyl-N'-nitrosourea-induced and spontaneous HER-2/neu transgenic mouse models of breast cancer. At a dose of 400 μg (100 μg per duct), drug levels (10.4 μmol/L) peaked after 24 hours, but when the same dose was administered by the intravenous route, drug concentrations (103.7 μmol/L) peaked at 4 hours. Compared to the intravenous route, the

intraductal administration of PLD resulted in substantially lower systemic exposure with no evidence of systemic toxicity or long-term histopathologic changes in the mammary gland. In addition, clinical studies had been conducted to prove the feasibility of the intraductal approach to treat breast cancer. Love *et al.* [92] investigated and demonstrated the safety of intraductal administration of PLD and carboplatin in women prior to mastectomy in a phase I clinical trial with the results suggesting that the administration technique is viable. Therefore the intraductal approach offers local targeting for treating DCIS.

Love et al. [92] also reported the rapid diffusion of carboplatin (t_{max}: ~30 min) out of the duct and into the systemic circulation and a delayed peak plasma concentration of PLD (t_{max}: >36 hr). The delayed DOX concentration was likely due to the controlled release of DOX from the PLD. In our studies, the inherent fluorescence of DOX (MW = 540 Da) facilitated the detection in mammary glands allowing for the estimation of ductal retention via non-invasive imaging. After intraductal administration, it exhibited a short retention half-life in mammary glands with a $t_{1/2}$ of 1.97 ± 0.35 hr. Given the rapid diffusion out of the duct, we sought to improve the retention of DOX by conjugating it to PEG nanocarriers. We further investigated the influence of molecular weight and structure on mammary gland retention. The PEG polymers of varying molecular weights (5, 10, 20, 40 kDa) and structures (linear, four-arm and eight-arm) were covalently attached to DOX via stable amide bond.

PEG was selected for the current studies because it is a polymer made of chemically inert polyether backbone and has been widely used in various clinical applications by parenteral, topical and oral administrations [93]. The advantage of using PEGs is that they are water-soluble, non-toxic and biocompatible [74]. PEGylation is a process of covalently attaching proteins, peptides, or small organic molecules to PEG polymers [5]. Abuchowsky and co-workers first applied PEGylation to albumin and catalase to modify their pharmacokinetics [69, 70]. After PEGylation, the proteins exhibited increased solubility, greater stability, reduced immunogenicity, lower renal clearance, prolonged plasma half-life and decreased uptake by cells of reticuloendothelial system (RES) [74]. Several PEGylated proteins have been approved for clinical use [77, 94-97]. For example, Intron® was developed by attaching a 12 kDa linear PEG to the protein resulting in a 10-fold greater elimination half-life than unmodified interferon-alpha2b [96]. Typical PEGylation involves the covalent attachment of one PEG to one drug molecule. In the current strategy, we are attaching multiple copies of DOX to a single PEG. Hence, the term PEG nanocarrier is used to describe the current configurations.

All nanocarriers were intraductally administered to the number 4 nipple on the left side of normal SD rats, and the distribution in the mammary gland was monitored noninvasively by measuring the fluorescence from the injected site and a control site. The IVIS 100 imaging system, is a highly sensitive, low light-level system optimized for whole living animal imaging. It is capable of calculating the fluorescence intensity of regions of interest. The method is suitable for high throughput screening of polymer diagnostics and therapeutics in mammary gland. Since DOX possesses inherent fluorescence, the

detection of DOX nanocarriers retention in rat mammary glands was observable without additional fluorescence-labeling. The fluorescence intensity obtained from the duct was plotted against time to estimate the retention half-life (t1/2) of nanocarriers in mammary gland. The $t_{1/2}$ of linear 5, 20, and 40 kDa, four-arm40 kDa, eight-arm 40 kDa nanocarriers were 2.23±0.28, 3.59±0.61, 13.11±3.41, 14.91±5.60, 11.90±2.91 h, respectively. The $t_{1/2}$ of free DOX was 1.97±0.35 h, consistent with rapid clearance of small molecule agents from the mammary gland into the systemic circulation [92].

The pharmacokinetics of the nanocarriers were also studied. The plasma levels of the linear 5k, linear 40 kDa, four-arm 40kDa and eight-arm 40 kDa peaked in 1.67±0.58, 11.5±0.87, 32±6.93, 9.33±2.31hr, respectively, whereas the DOX reached C_{max} in 0.23±0.23 h. Therefore, PEGylation resulted into a delayed plasma peak time in a molecular-size dependent manner. These studies demonstrate that PEG-DOX nanocarrier ductal retention was directly related to DOX pharmacokinetics and delays in appearance in the systemic blood circulation.

The current results can be explained using the hydrodynamic radii data of PEG polymers as well. The hydrodynamic radii of linear 5, 10, 20, 40 kDa, four-arm and eight-arm 40 kDa were estimated as 2.661±0.161, 2.699±0.709, 4.521±0.681, 7.375±0.454, 6.199±0.403, and 5.622±0.389 nm, respectively. PEG displays coiled/extended conformation with large hydrodynamic radius. When it is fully hydrated, it coordinates 2-3 water molecules per ethylene oxide unit, leading to an increase in 5-10 times larger in their molecular weight than corresponding globular proteins of comparable mass [98].

Thus, hydrodynamic radii increased with increase in molecular weight for linear and branched polymers exhibited lower hydrodynamic radii than corresponding linear polymers of same molecular weight. Together with in vivo studies, ductal retention $t_{1/2}$ and plasma $t_{1/2}$ increased with increase in molecular weight of linear nanocarriers. At the same molecular weight of 40 kDa, the hydrodynamic radii decreased with an increase in branches of polymer structure.

In addition, we found inflammatory cells invasion and alteration of ductal structures in the SD mammary gland when we intraductally administered DOX. On the other hand, we did not observe any inflammation in the nanocarrier treated groups, implying less irritation in the local area. But DOX and nanocarrier treated groups all showed certain extent of stripping of ductal epithelial cells, suggesting PEG-DOX nanocarriers are potentially effective in treating cancer cells.

4.5 Conclusions

In conclusion, we studied the mammary gland retention of PEG-DOX nanocarriers of different molecular weight (5, 10, 20 and 40 kDa) and structure (linear, four-arm and eight-arm) by non-invasive approach. The PEG-DOX nanocarriers showed significantly prolonged mammary gland retention with respect to the DOX, which showed extremely short retention.

The estimation of retention half-lives revealed that retention of nanocarriers in mammary gland was influenced by not only the polymer molecular weight but also structure. For

both linear and branched nanocarriers, retention in mammary glands increased with increase in molecular weight, and for nanocarriers of same molecular weight, retention decreased with increase in branching in polymer structure. The only exception was four-arm 40 kDa nanocarrier, which showed higher retention than corresponding linear and eight-arm nanocarriers, probably due to the nanocarrier permeation through mammary gland. Plasma distribution studies revealed that higher the nanocarrier retention in mammary gland, the more delayed is the plasma peak time. This study conclusively shows that molecular size can be used to improve the retention of low molecular weight therapeutic agents in breast mammary gland. The data present here will aid in the design of delivery systems for intraductal diagnostics and therapy to locally target breast ducts.

4.6 Acknowledgment

This work was supported by the grants from Windy Hill Medical, Inc., CA and National Institutes of Health HIT IT (R01AI084137-01). We also thank Prof. Arash Hatefi at Rutgers Department of Pharmaceutics for giving us access to Malvern Zetasizer Nano ZS.

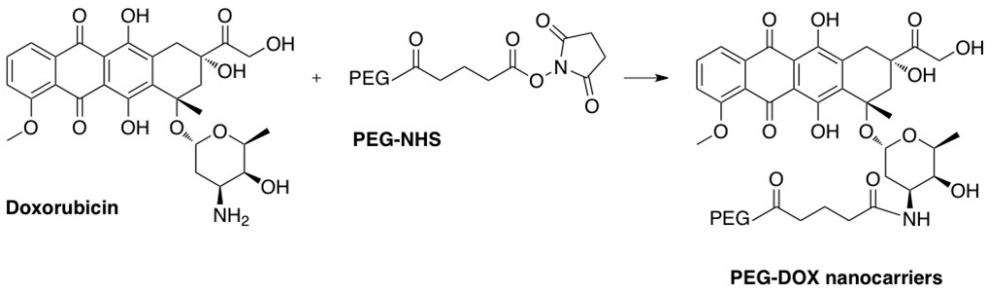

Scheme 4.1. Synthesis of PEG-DOX nanocarriers. The nanocarriers of different molecular weight and structure were prepared by reacting PEG-NHS with DOX. Reagents and Conditions: DIEA/DMF, room temperature, stir for 6 hours.

Table 4.1. Purity of PEG-DOX nanocarriers

Nanocarriers	**Purity**
5 kDa PEG-DOX	98.9%
10 kDa PEG-DOX	99.5%
20 kDa PEG-DOX	99.4%
40 kDa PEG-DOX	99.6%
40 kDa PEG-$(DOX)_4$	98.0%
40 kDa PEG-$(DOX)_8$	99.3%

Table 4.2. DOX-loading of PEG-DOX nanocarriers

Nanocarriers	**DOX-loading (w/w)**
5 kDa PEG-DOX	3.3%
10 kDa PEG-DOX	3.0%
20 kDa PEG-DOX	2.1%
40 kDa PEG-DOX	1.0%
40 kDa PEG-$(DOX)_4$	2.2%
40 kDa PEG-$(DOX)_8$	4.5%

Table 4.3. Hydrodynamic radii of PEG polymers measured using Dynamic Light Scattering

PEG polymers (Mw in kDa)	**Hydrodynamic radii in nm (mean ±SD, n=5)**
Linear 5 kDa PEG	2.661 ±0.161
Linear 10 kDa PEG	2.699 ±0.709
Linear 20 kDa PEG	4.521 ±0.681
Linear 40 kDa PEG	7.375 ±0.454
Four-arm 40 kDa PEG	6.199 ±0.403
Eight-arm 40 kDa PEG	5.622 ±0.389

Table 4.4. Cytotoxicity of PEG-DOX nanocarriers against MCF-7 cell line

Nanocarriers and DOX	**IC50 (95% CI) (μM)**
DOX	0.14 (0.12/0.16)
5 kDa PEG-DOX	1.76 (1.62/1.92)
10 kDa PEG-DOX	3.86 (3.44/4.34)
20 kDa PEG-DOX	8.96 (7.51/10.69)
40 kDa PEG-DOX	18.11 (12.28/26.70)
40 kDa PEG-$(DOX)_4$	1.23 (1.11/1.36)
40 kDa PEG-$(DOX)_8$	3.49 (3.05/3.98)

Table 4.5. Retention half-lives of PEG-DOX nanocarriers in mammary gland of female SD rats

Nanocarriers and DOX[a,b,c]	**$t_{1/2}$ (h, mean ±SD, n=3)**
DOX	1.97 ±0.35
5 kDa PEG-DOX	2.23 ±0.28
20 kDa PEG-DOX	3.59 ±0.61
40 kDa PEG-DOX	13.11 ±3.41
40 kDa PEG-$(DOX)_4$	14.91 ±5.60
40 kDa PEG-$(DOX)_8$	11.90 ±2.91

[a] $t_{1/2}$ is defined as time at which fluorescence reaches 50% of its original value

[b] $t_{1/2}=\ln 2/K_{el}$, where K_{el} is the elimination rate constant

[c] K_{el} is calculated by regression of semi-logarithmic fluorescence *vs.* time data: $\ln F = \ln b - tK_{el}$.

Table 4.6. Pharmacokinetic parameters of PEG-DOX nanocarriers in plasma

Nanocarriers and DOX[a,b,c]	**$t_{1/2}$ (h, mean ±SD, n=3)**	**t_{max} (h, mean ±SD, n=3)**	**c_{max} (mg/ml, mean ±SD, n=3)**
DOX	1.70 ±1.28	0.23 ±0.23	0.0000161 ± 4.63e-6
5 kDa PEG-DOX	11.4 ±5.25	1.67 ±0.58	0.0036 ±0.00047
40 kDa PEG-$(DOX)_4$	104 ±41.1	32.0 ±6.93	0.035 ±0.00080
40 kDa PEG-$(DOX)_8$	56.5 ±28.7	9.33 ±2.31	0.096 ±0.028

[a] $t_{1/2}$ is defined as time at which fluorescence reaches 50% of its original value

[b] $t_{1/2}=\ln 2/K_{el}$, where K_{el} is the elimination rate constant

[c] K_{el} is calculated by regression of semi-logarithmic fluorescence *vs.* time data: $\ln F = \ln b - tK_{el}$.

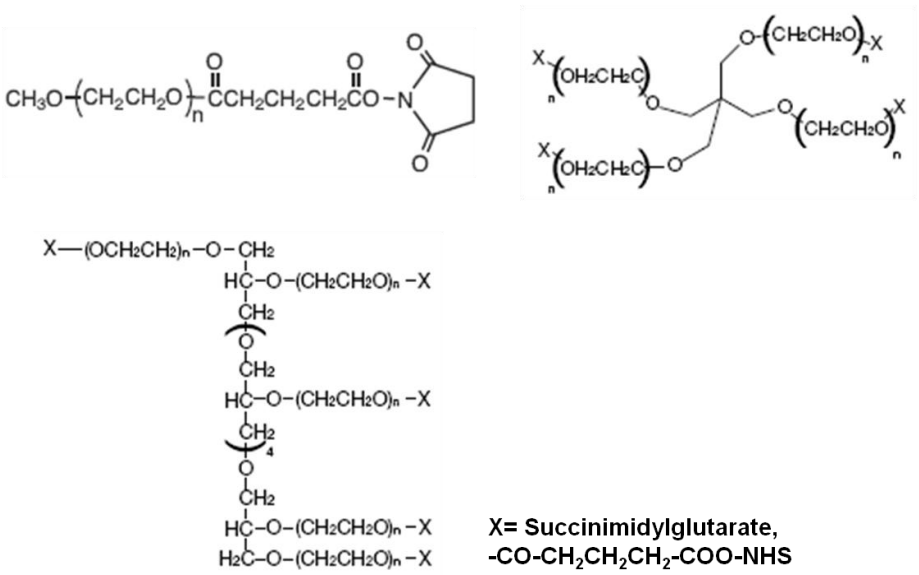

Figure 4.1. Structures of the PEG polymers with different molecular weight (5, 10, 20, and 40 kDa) and structure (linear, four-arm and eight-arm)

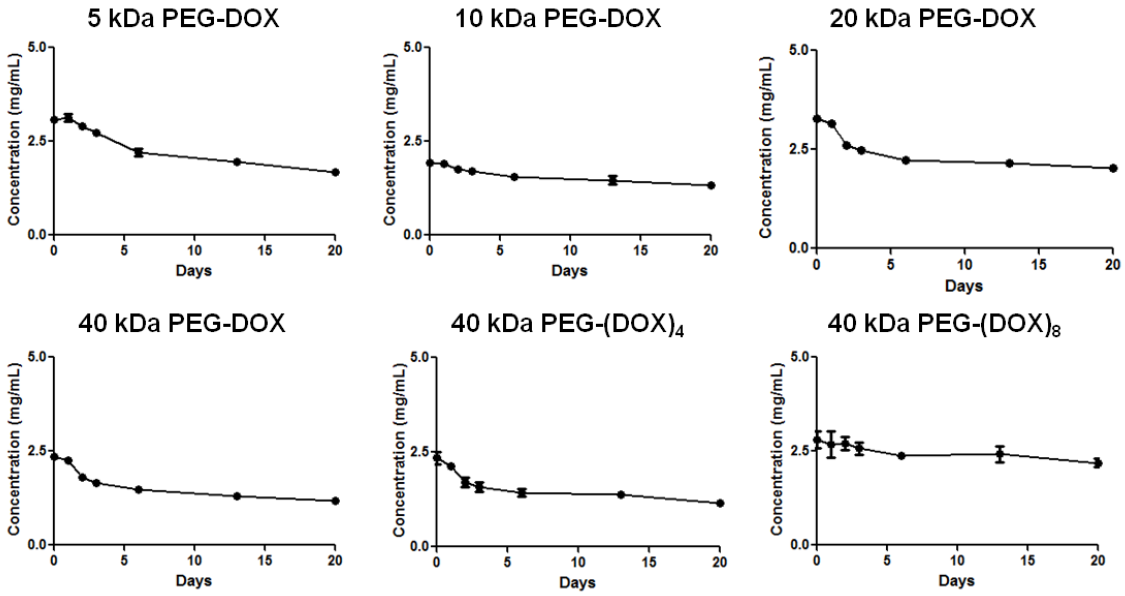

Figure 4.2. Amide bond stability of PEG-DOX nanocarriers in 0.1 M Sodium phosphate buffer (pH 7.4) at 37 ℃ separately for 20 days: (A) 5 kDa PEG-DOX; (B) 10 kDa PEG-DOX; (C) 20 kDa PEG-DOX; (D) 40 kDa PEG-DOX; (E) 40 kDa PEG-$(DOX)_4$; (F) 40 kDa PEG-$(DOX)_8$. Mean ±SD, n=3.

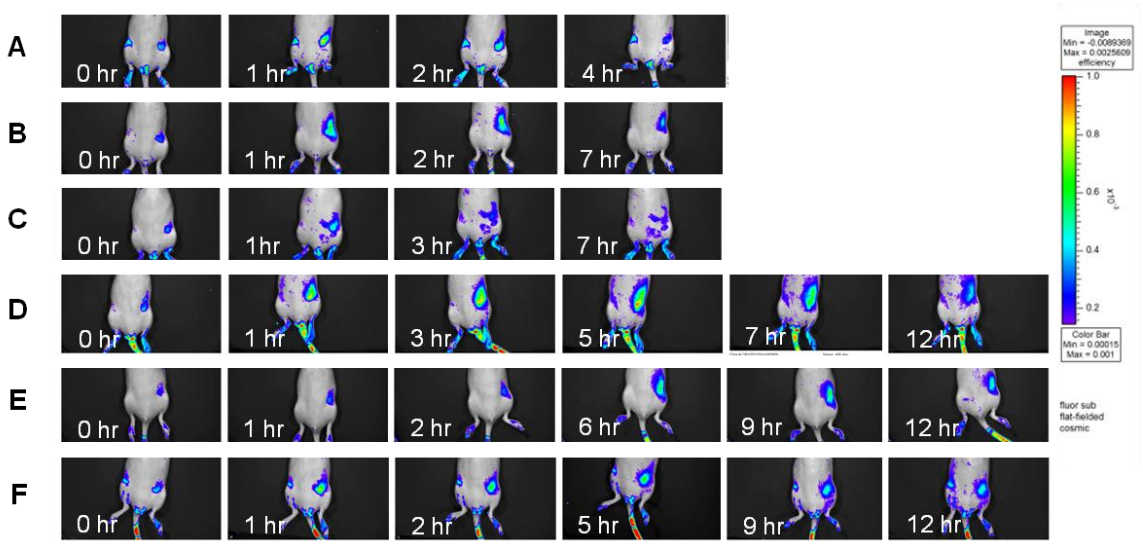

Figure 4.3. Retention of PEG-DOX in mammary gland: (A) DOX; (B) 5 kDa PEG-DOX; (C) 20 kDa PEG-DOX; (D) 40 kDa PEG-DOX; (E) 40 kDa PEG-$(DOX)_4$; (F) 40 kDa PEG-$(DOX)_8$. The solutions for injection (0.83 mg/kg/duct) were prepared and administered intraductally into the teat of SD rats (n=3). Animals were imaged at different time points on an IVIS® 100 system.

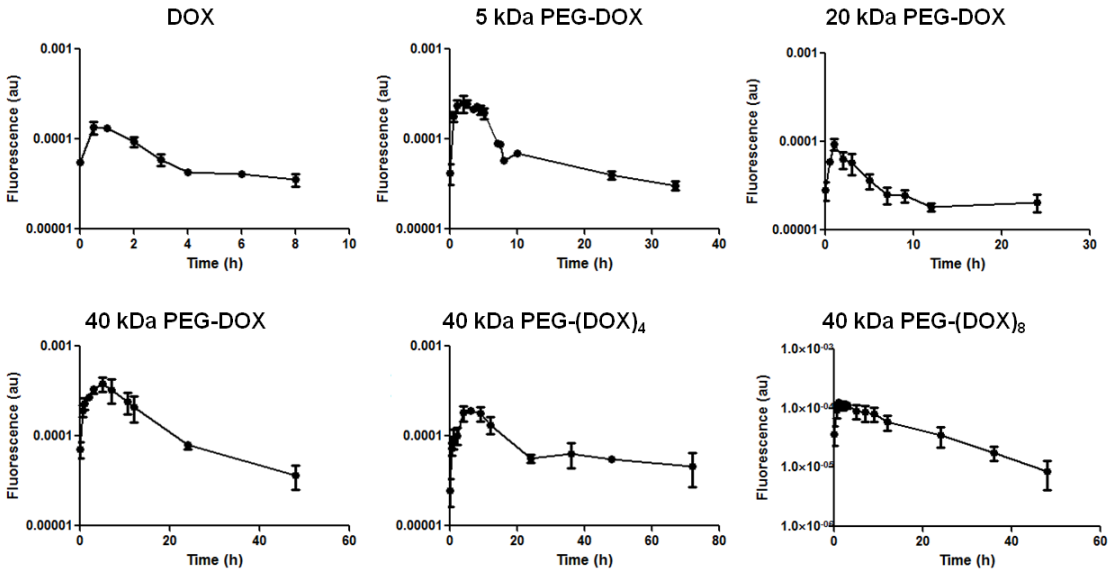

Figure 4.4. Distribution of PEG-DOX nanocarriers in mammary gland. PKSolver was used to estimate $t_{1/2}$ by non-compartmental analysis, and each data point represents mean ±SD (n = 3).

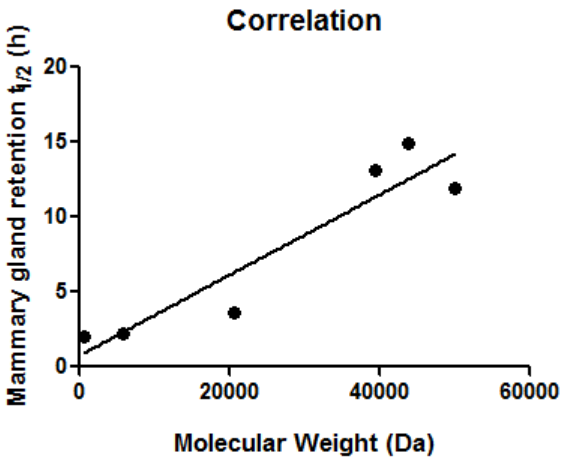

Figure 4.5. Correlation between molecular weight and mammary gland retention half-life. R^2= 0.7308.

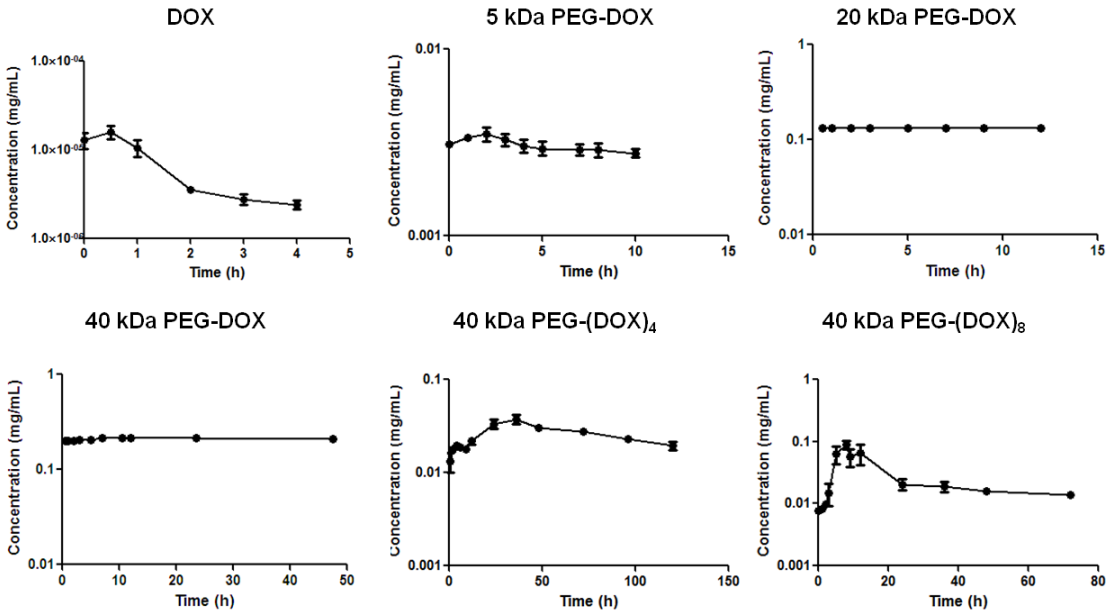

Figure 4.6. Pharmacokinetics parameters of PEG-DOX nanocarriers in plasma. Plasma levels were measured using RP-HPLC with UV and fluorescence detector. The results were normalized with nanocarrier standard curve in plasma. Each data point represents mean ±SD (n = 3).

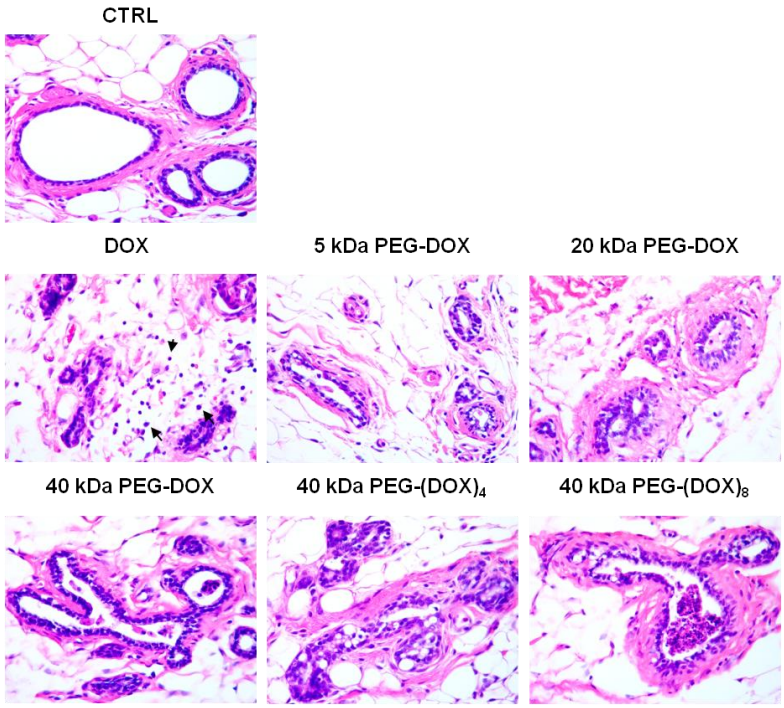

Figure 4.7. Histological studies of mammary glands treated with DOX and nanocarriers (0.83 mg/kg DOX equivalent). Rats were euthanized after 6 days of dosing. Hematoxylin and eosin (H&E) stained sections. Thickness: 5 μ .

5 A NOVEL ORTHOTOPIC DUCTAL CARCINOMA IN SITU (DCIS) BREAST CANCER MODEL IN RATS BY NONINVASIVE INOCULATION

5.1 Introduction

Breast cancer is the most common type of cancer among women in the world [11, 12]. In US, one in eight women will be diagnosed with invasive breast cancer over the life time course [13]. And approximately 232,340 new cases of invasive breast cancer and 39,620 breast cancer deaths are expected to occur among US women in 2013 [13]. The five-year survival rates for noninvasive and locally invasive breast cancers are 98% and 83.3% respectively, however the rates for cancers that have spread to distant sites decrease to 27.1% significantly [10]. In addition, noninvasive early stage breast cancer has been shown to be associated with an increased risk to develop invasive cancer based on laboratory and patient data [33-35]. Therefore early diagnosis followed by efficient intervention is the key to improve patient survival rate.

To well study the development of breast cancer, especially the early stage, several rodent breast cancer models have been established. 1-Methyl-1-nitrosourea (MNU) model, developed by Thompson et al. [7], is a carcinogen induced breast cancer model. It provides rapid induction of premalignant and malignant stages of mammary carcinogenesis by i.p. injection of MNU into female Spargue-Dawley (SD) rats at 20 days of age [7]. Limitation of this model is noninvasive lesions may develop in any 12 mammary glands of the rats. Therefore it requires treatment to all the mammary glands,

which is time, labor and cost-inefficient. Another frequently used model is subcutaneous (heterotopic) model. This model is very convenient, but a potential disadvantage for the subcutaneous model is the cancer cells are not orthotopically inoculated, leading to a low take rate with a widely varied percentage, depending on the type of cancer [8, 9]. Moreover, the tumor is initiated in the subcutis, which may have potential influence of the biology of the subcutis on the tumorigenicity. Furthermore, it may lack the consistent invasive and metastatic behavior. Due to these limitations, orthotopic models have been developed by inducing the tumors in organ of origin in the laboratory animals. It can significantly increase the take rate of tumors and occasionally facilitate metastatic spread that will not occur in s.c.model [84, 85]. Behbod et al. [10] established an intraductal human-in-mouse transplantation model. This model gave high take rates (90%), with initial human DCIS cell (MCF10DCIS.COM and SUM-225 cell line) growth confined within the mammary ducts, followed by progression to invasion in some cases into the stroma. The DCIS-like lesions were found by 6 weeks after injection. However the teat of mice is really tiny to inject. In their experiments, they made a Y-incision to expose the inguinal gland and the nipple was cleaved for the convenience to put the 30 G needle directly into the ducts. Though this model mimics the heterogeneity at the noninvasive stages, it takes long time to develop DCIS lesions and the approach is invasive and time-consuming.

In our minds, an ideal model should faithfully reflect that the tumor grows and proliferates in the mammary duct with a 100% incidence. And it should provide proper time period of lesion development. Finally it would achieve at an acceptable level of

experimental convenience and cost. Our laboratory has developed and characterized an orthotopic breast cancer model in F344 rats using a non-invasive intraductal approach. The 13762 Mat B III cells were noninvasively introduced into the left four position of mammary duct in F344 female rats, thus mimicking the development of non-invasive lesions in its normal environment. In this report, we describe the development and characterization of this breast cancer model. It allowed us to follow the natural progression of human breast cancers, i.e., their initial growth as carcinoma in situ inside the ducts, sometimes followed by invasion into the stroma by overcoming the barriers of an intact myoepithelial cell layer and a basemen membrane. Therefore this model could be a very useful experimental system for preclinical studies and treatment of breast cancer.

5.2 Materials and methods

5.2.1 Cell line

The 13762 Mat B III cells (American Type Culture Collection), a rat mammary adenocarcinoma cell line, were maintained in RPMI 1640 medium supplemented with 10% fetal bovine serum (FBS) and 10 % penicillin/streptomycin under condition of 5% CO_2 and 95% humidity at 37 ℃.

5.2.2 Animals

Female Fischer 344 rats (F344) (young virgin rats (6-8 weeks of age) and retired breeders) were obtained from Hilltop Lab Animals, Inc (Scottdale, PA). The Principles of

Animal Care by the National Institutes of Health (NIH) and a protocol approved by the Rutgers University Institutional Animal Care and Use Committee were used to perform animal experiments. The animals were housed in Rutgers Laboratory Animal Services facility accredited by the Association for the Assessment and Accreditation of Laboratory and Care International (AAALAC), and maintained on a 12-h light/dark cycle in a temperature-controlled environment, with food and water *ad libitum*. After acclimatization for one week, rats were subjected to intraductal injection with cancer cells.

5.2.3 Intraductal inoculation

Female F344 rats were anesthetized with isoflurane and placed under a dissection microscope. The number four nipple on the left side was cleaned with 70% ethanol. After the dilation of the orifice, 13762 Mat B III cells in serum-free RPMI medium were inoculated intraductally into the left fourth teat using a 33 G needle attached to a Hamilton syringe (Hamilton, Reno, NV).

5.2.4 Establishment of orthotopic model

Several studies were performed to evaluate establishment of cell inoculation into the mammary duct non-invasively.

5.2.4.1 Establishment of orthotopic model in F344 young virgin rats

At day 0, 20×10^4 13762 Mat B III cells transfected with EGFP were administered intraductally into left number four teat of F344 young virgin rats. The live rat body images were taken on an IVIS® 100 optical imaging system after 14 days of the initial cell inoculation. The following instrument settings were used: Level: High; Em: GFP; Ex: GFP; Bin: hr (4), FOV25, Aperture: f2, and shutter: 1s. Mammary whole mounts was prepared by excising the abdominal-inguinal mammary gland at day 3 for further examination under fluorescence microscopy at $25\times$ magnification. At day 21, developed mammary tumors were excised and embedded into OTC compound. The prepared tumor cryosection was observed under fluorescence microscope at $100\times$ magnification.

5.2.4.2 Establishment of orthotopic model in F344 retired breeders

13762 Mat B III cells (cell load: 25×10^4) were injected intraductally into F344 retired breeders. After 10 days of cell inoculation, rat body images were acquired with a 1T M2 High Performance MRI System (Aspect Magnet Technologies Ltd, Netanya, Israel). Two scans were taken, one covering the lower body starting at the duct, the other covering the upper torso. All scans were run at a 256-250 matrix, with the TE/TR at 80/3787 and a Flip Angle of 180 degrees. Five averages (with each average improving the image quality) were taken each time. The data was transferred from the MRI to an analysis software program Vivoquant. In Vivoquant the images were reviewed to look for any activity (tumors or fluid, fibrosis or irritation, metastasis). Images were compared to the prior scans (self-control) to compare growth or activity.

5.2.5 Tumorigenicity of 13762 cells in F344 rats

Followed cell inoculation, all rats were monitored for tumor progression by palpation and observation of their physical health, appearance and body weight every 2-3 days. Animals were euthanized by CO_2, when they developed tumors that reached a size of approximately 40×40 mm. Tumor, lung, liver, spleen, axillary lymph nodes were collected and fixed in 10% buffered neutral formalin for further analysis.

5.2.6 Preparation of mammary whole mount

The rats were euthanized at different days after the intraductal inoculation of 13762 Mat B III cells. The abdominal-inguinal mammary glands were excised and fixed in 10% neutral formalin for 24 hours and then rinsed in distilled water for 15 min. The glands were then dehydrated in a serial concentration of ethanol (70%, 95%, and 100%) for 1 hour each and defatted in two changes of xylene for 1 hour each, followed by rehydration and immersing in carmine alum-staining solution. One week later, the stained whole mounts were dehydrated using serial concentration of ethanol as described above, cleared in xylene for 2 hour and stored in biopsy pouches filled with methyl salicylate. The whole mounts were left overnight and the next day residual air bubbles were removed by tapping the pouch. All whole mounts were photographed at uniform magnification. Lesions are identified on the photograph. Thereafter, all detectable lesions are dissected from the whole mount.

5.2.7 Histological studies

The detectable lesions are dissected from the whole mount and placed in individual tissue-processing cassettes. The cassettes are processed through three changes of toluene to remove residual methyl salicylate and then infiltrated with molten paraffin. The infiltrated specimens were then embedded into paraffin blocks, which were sectioned to 5-micron thickness and mounted onto glass slides. The tissue slides were stained using hematoxylin and eosin (H&E) protocol.

5.2.8 Data analysis

Experimental values were expressed as mean ± standard error (SE). Statistical significance was considered if p value was < 0.05.

5.3 Results

5.3.1 Establishment of orthotopic model by intraductal route

With the idea that most breast cancer initiates and grows inside the ducts, we directly inoculated 13762 Mat B III cells into the primary ducts to initiate the tumor growth in mammary ductal environment. Since 13762 Mat B III cell line is a cell line derived from Fisher 344 rat-derived mammary adenocarcinoma, this developed model is a syngeneic model.

To firstly explore whether the tumors were successfully initiated in the mammary duct, 13762 Mat B III cells transfected with EGFP was used to define the location of cells injected in young virgin rats. We took rat body images at day 10 by IVIS®100 imaging system. The fluorescence signal in the left number four position was recorded (Figure 5.1).

In our serial studies under fluorescent microscopy, green fluorescence from EGFP was observed in the mammary gland whole mount, which was excised after 3 days of cell inoculation, while no fluorescence signal was obtained from the control whole mount, indicating the cells were growing in the mammary glands (Figure 5.2). The fluorescence signal was also observed in tumor cryosection which was prepared from the harvested tumor after 21 days of cell inoculation (Figure 5.3). Moreover, we tested the feasibility of intraductal inoculation in retired breeders by applying MRI scanning. After 10 days of cell inoculation, tumors were found in abdominal-inguinal mammary gland (Figure 5.4). All these results suggest the successful inoculation of cells in the mammy glands in both F344 young virgin and retired breeder rats.

5.3.2 Tumorigenicity of 13762 cells in F344 rats

The take up rate of 13762 Mat B III cells on both young virgin and retired breeder rats was 100% for all tested cell load groups. Once the mammary tumors were palpable, the development of tumors was fast. A cell load dependent manner was observed in both young virgin rats and retired breeders. When a higher cell load was administered, the tumor developed more rapidly with respect to lower cell load groups (Figure 5.5).

In Figure 5.6, it is interesting to note that the tumor volume of young virgin rats injected with 5×10^4 cell load was larger than the tumor volume of retired breeders injected with 25×10^4 cell load at all recorded time points. In addition, histological studies exhibited extensive metastases to distal organs were observed in young virgin rats (Figure 5.7), while no metastases were found in retired breeders. All these results indicate that young virgin rats are more susceptible to 13762 Mat B III cells than retired breeders, which are in consistence with human beings. In human, the risk of developing breast cancer is largely associated with reproductive factors, including nulliparity, late age at first birth and recent use of postmenopausal hormone therapy [21]. Specifically the risk is reduced by higher parity and lactation [21].

5.3.3 Early stage lesions define

We inoculated 0.5×10^4, 1×10^4, and 2×10^4 cell loads on young virgin rats and euthanized the rats at day 3, 6 and 9. As exhibited in Figure 5.8, on day 3, no darkened spots were observed among all three cell load groups. Starting from day 6, darkened spots were observed among all groups. When we increased the cell load, the size and number of dark spots increased at the same time points, showing a cell load dependency. At the same cell load group, as time passed, the size and number of lesions increased, indicating a time dependent manner in young virgin rats. The time dependent manner was also found out in the whole mounts from retired breeders with inoculation of 25×10^4 cells (Figure 5.9).

The histology of premalignant and malignant lesions in both young virgin and retired breeder rats was presented too. In young virgin rats inoculated with lower cell loads, most mammary gland ducts looked normal and some exogenous cells (probably injected cancer cells) in lumen, epithelial cell mitosis and micro cancerous alteration were presented. In higher cell load groups, more frequently epithelial cell alteration with mitosis was observed. As time went by, tumor cells invaded the ductal wall and grew outside of ducts, along with developed low grade DCIS and solid type DCIS (Figure 5.10). Histology from retired breeders showed that DCIS lesions developed after 2 days of 25×10^4 13762 Mat B III cell inoculation (Figure 5.11). Based on the cancer cell growing pattern in both young virgin and retired breeder rats, tumorigenicity of 13762 Mat B III cells shows time-dependent and cell load-dependent manner.

5.4 Discussion

There are several established breast cancer models aimed to provided a great deal of insight about many factors involved in the prevention and treatment of breast cancer, for example, MNU model [7], subcutaneous model and HIM model [10]. However, we believe that our model offers several advantages over most of the currently established breast cancer models.

Firstly, an important feature of this model is the application of an intraductal approach. In our studies, we inoculated the 13762 Mat B III cells directly into mammary ducts via a blunt-ended needle, thus providing initial growth of carcinoma in the natural microenvironment instead of in the subcutaneous tissue or fat pads, followed by invasion

into the stroma by overcoming the barriers of an intact myoepithelial cell layer and a basement membrane, which allow us to follow the natural progression of breast cancer. Moreover, the way to inoculate cells is totally non-invasive. In reported HIM model [10], a significant injury was associated with making a Y-incision on the abdomen to expose the inguinal mammary fat pad and administer tumor cells via clipped nipple. The approach to establish HIM model is really invasive and likely cause inflammation. Meanwhile it takes a lot of time to finish procedures in one mouse. While in our studies, we used rats as experimental rodents to facilitate the injection under the dissection scope due to the ten-fold larger animal size and larger teat with respect to mice, making this approach technically feasible and non-invasive.

Secondly, based on the cell load applied, the early stage lesions can be confined within the mammary duct with no invasion for around 7-9 days, making this model a valuable tool to study the early stage breast cancer. Moreover, the progressive primary tumor growth was observed in this model, cause eventual cancer-related morbidity, thus making survival a feasible study endpoint.

Finally, the 13762 Mat B III cell line used was derived from adenocarcinoma in F344 rats, making this model a syngeneic *in vivo* model of breast cancer. This model gives very high (100%) take rate and consistent growth rate, resulting in few wasted animals. And developed mammary tumors grow rapidly, requiring only four to five weeks for a complete study. Furthermore, our F344 model facilitates efficacy study by administering anti-cancer agents to the mammary gland where we induced tumor before, while MNU

model requires treatments to all 12 mammary glands because the mammary tumor may develop in any 12 mammary glands [7].

In our studies, we used both young virgin female rats and retired breeders. The results showed development of mammary tumor in cell-load and time dependent manner. We noted that the retired breeders required higher cell load to initiate the early stage non-invasive lesions with respect to the young virgin rats. In addition, metastasis was only observed in the young virgin rats. The results suggest young virgin rats are more susceptible to 13762 Mat B III cells than retired breeders, which is corresponded well to human beings. In women, besides of age, sex, and family history of breast or ovarian cancer, risk of developing breast cancer is largely associated with reproductive factors, including nulliparity, early menarche, late menopause, and late age at first birth [15-17, 21]. Specifically, risk of developing breast cancer is increased by early menarche, late menopause, and nulliparity, whereas, risk is reduced by higher parity and lactation [99]. So incidence of getting breast cancer in young nulliparous women is higher than in women after lactation. Since in our model, young virgin rats were more susceptible to develop mammary tumors than retired breeders at the same cell load, it indicates our model has some clinical relevance.

Rodent models are informative in the absence of human data. They have provided valuable information on the dose and route of administration to be used and optimal host conditions for eliciting maximal tumorigenic response. However our model has its own limitations. 13762 Mat B III cell line is not a human cell line. It may not mimic the

human breast cancer progression type well. In addition, after a couple days of cell injection, we can see the cells piled up in the lumen, which is artificial for the tumor development.

Overall, this method is efficient, convenient and cost-effective. It gives very high (100%) take rate and consistent growth rate. This model should be particularly useful as a preclinical model.

5.5 Conclusions

The significance of this study is the establishment of a novel model using noninvasive intraductal approach. This model offers a ductal microenvironment for primary tumor growth, and is highly relevant to human breast cancer. Therefore it makes further efficacy studies using this model extremely pertinent.

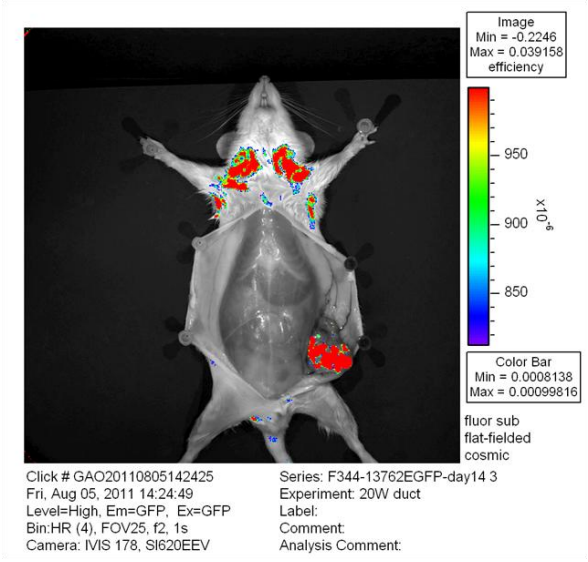

Figure 5.1. Body image of a female F344 young virgin rat inoculated with 13762 Mat B III cell line transfected with EGFP. This rat was euthanized after 14 days of initial inoculation of 20×10^4 cells. Abdominal-inguinal mammary gland was exposed for imaging on an IVIS® 100 imaging system.

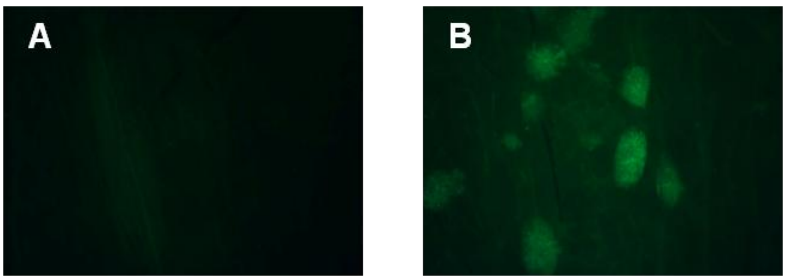

Figure 5.2. Mammary whole mount of female F344 young virgin rats. (A) mammary gland from rat without cell inoculation (control); (B) mammary gland from rat injected with 13762 Mat B III cell line transfected with EGFP (cell load: 20×10^4). Rats were euthanized after 3 days of cell inoculation. Mammary glands were excised and whole mounts were prepared and observed under fluorescence microscope using ×25 magnification.

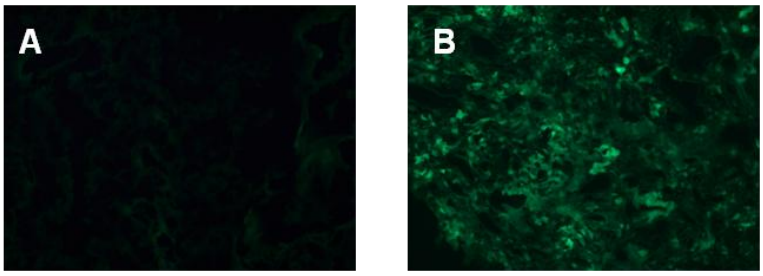

Figure 5.3. Tumor cryosection from female F344 young virgin rats: (A) 13762 Mat B III cells without transfection; (B) 13762 Mat B III cells transfected with EGFP. Female F344 young virgin rats were intraductally administered with 20×10^4 13763 Mat B III cells with or without transfection. At day 21, the rats were euthanized. The developed tumors were excised and prepared for tumor cryosection which were examined under ×100 magnification.

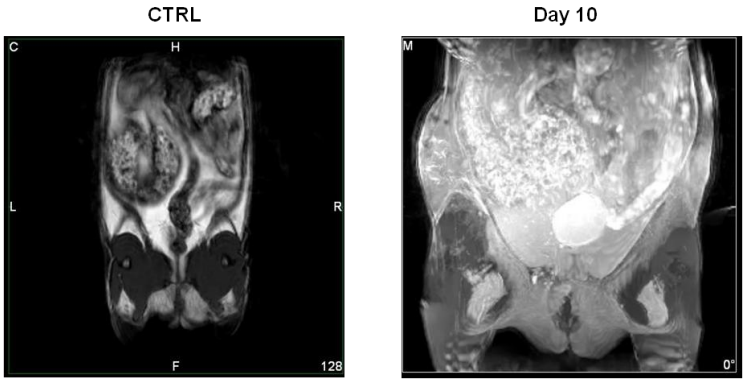

Figure 5.4. MRI images from F344 retired breeders. MRI image was taken before the cell inoculation (self-control). The rats inoculated with 25×10^4 13762 Mat B III cells were imaged at different days by MRI scanning.

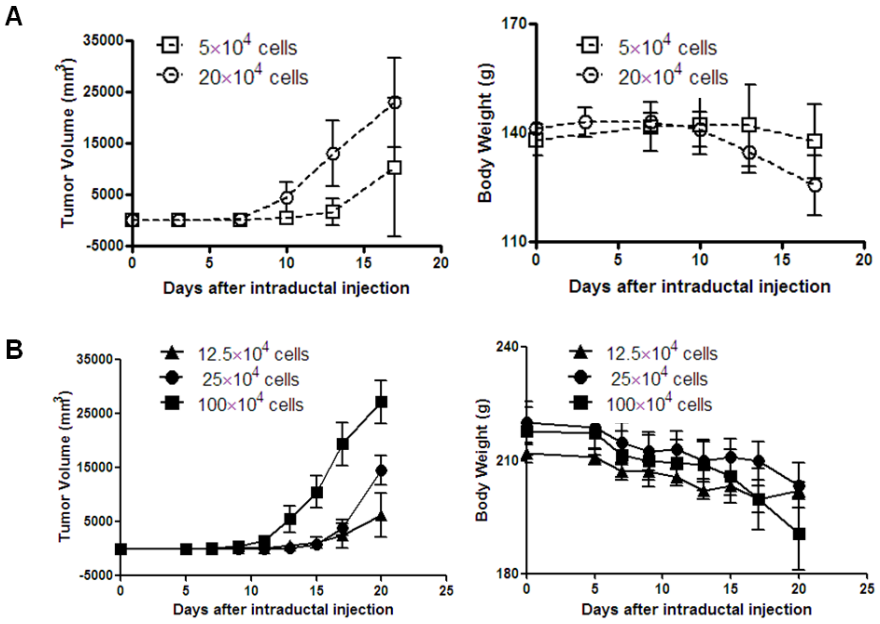

Figure 5.5. Tumorigenicity of 13762 cells in F344 rats: (A) young virgin rats; (B) retired breeders. Each point represents the mean ± SE (n=3-4). The rats were intraductally inoculated with different cell loads. Tumor volume and body weight were recorded at given time points.

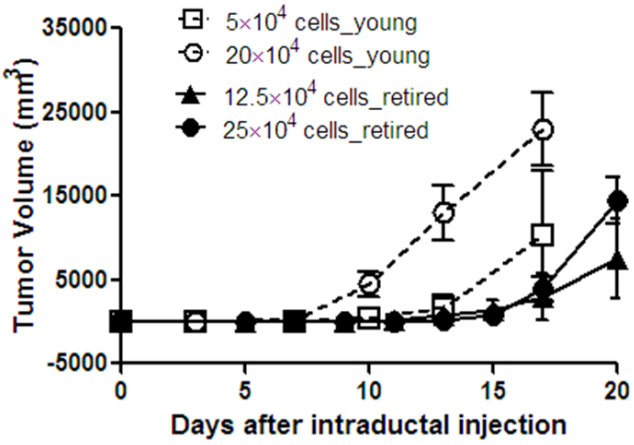

Figure 5.6. Tumor volume growth in young virgin rats and retired breeders. Each point represents the mean ± SE (n=3).

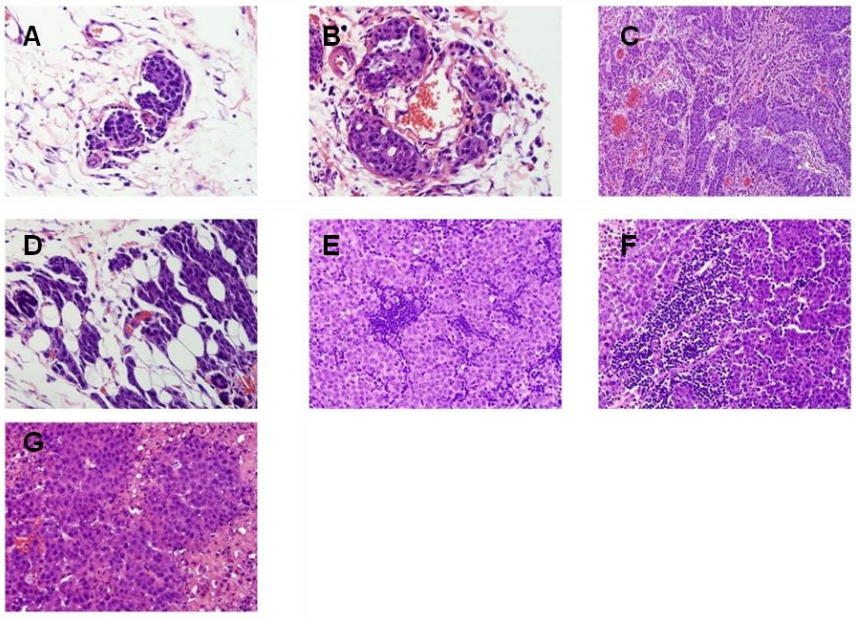

Figure 5.7. The intraductal inoculation breast cancer model manifested extensive metastasis to distal organs. (A) tumors in vein, day 17; (B) tumors surrounding a vein, day 17; (C) axillary metastasis, day 23; (D) mammary gland, day 17; (E) mammary lymph node, day 17; (F) peritoneal lymph node, day 21; (G) primary tumor, day 17. Microscopic images were taken at 40x objective. Cell load: 5×10^4, thickness: 5 μ. Microscopic images were taken at $\times 40$ objective.

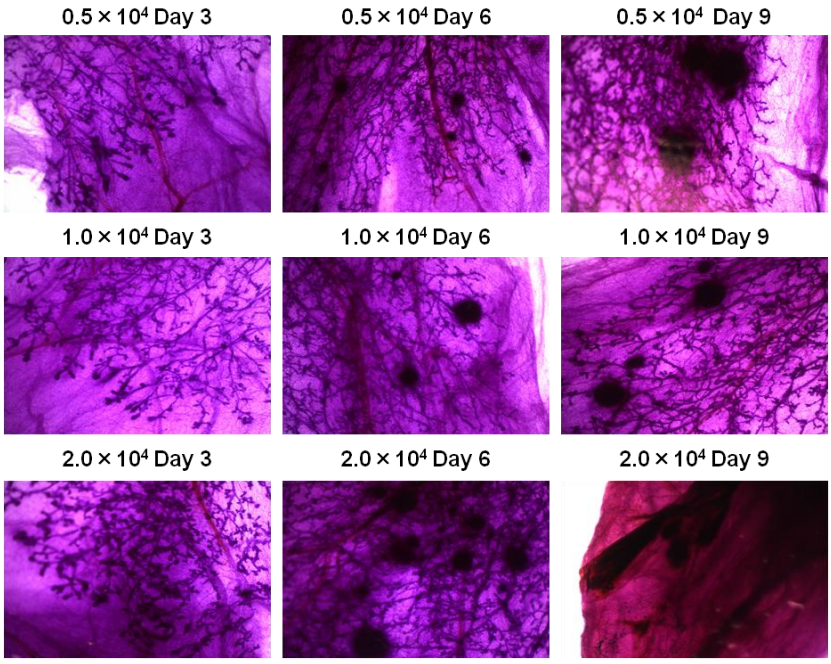

Figure 5.8. The sub-gross and histological appearance of mammary gland duct from F344 female young virgin rats. Subgross photomicrographs are from alum carmine stained mammary gland whole mounts. Microscopic images were taken at ×0.65 objective.

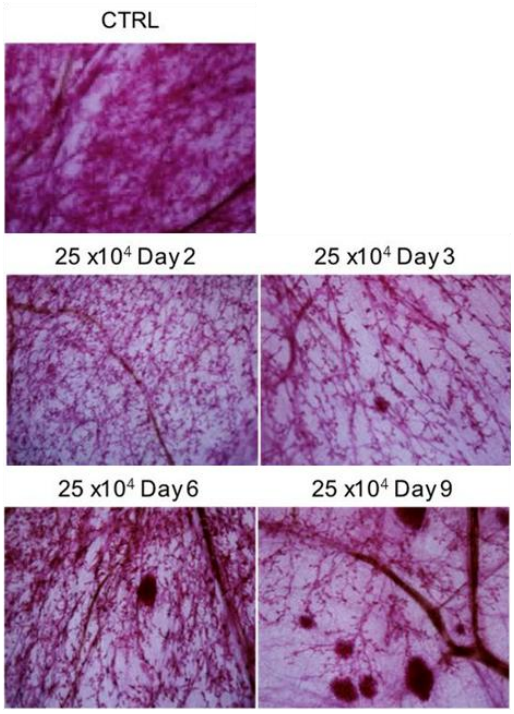

Figure 5.9. The sub-gross and histological appearance of mammary gland duct from retired breeders inoculated with 25×10^4 13762 Mat B III cells. Subgross photomicrographs are from alum carmine stained mammary gland whole mounts. Microscopic images were taken at ×2 objective.

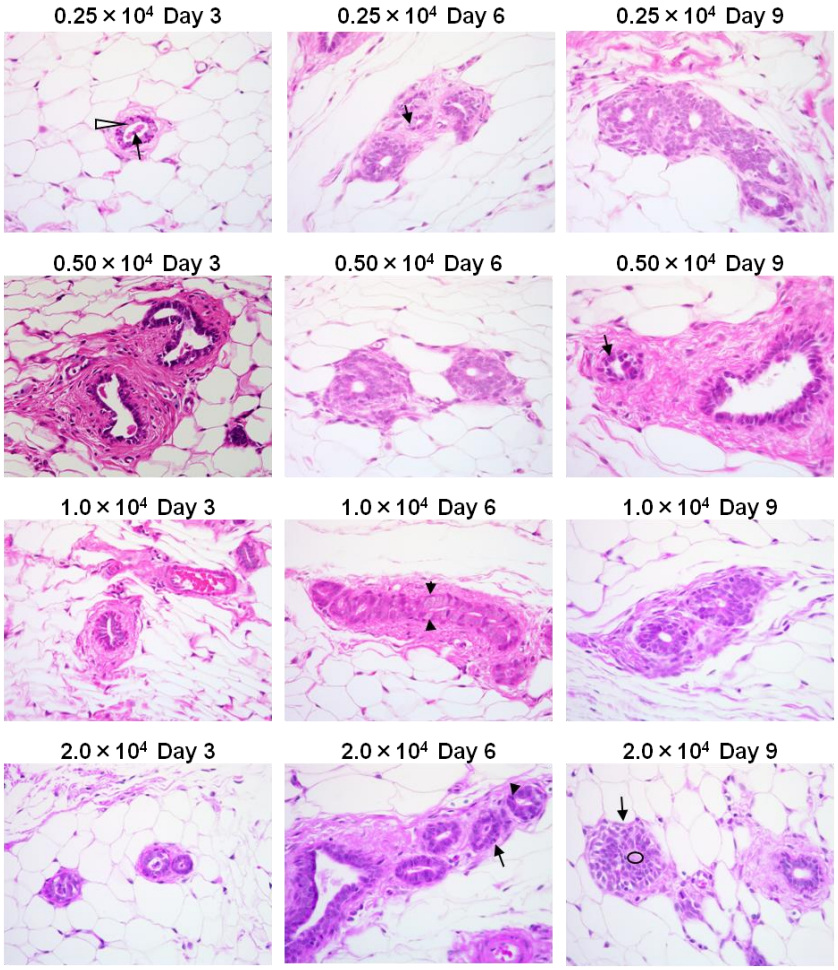

Figure 5.10. H & E staining to study early lesions in mammary ducts from F344 female young virgin rats. Microscopic images were taken at ×40 objective. Thickness: 5 µ.

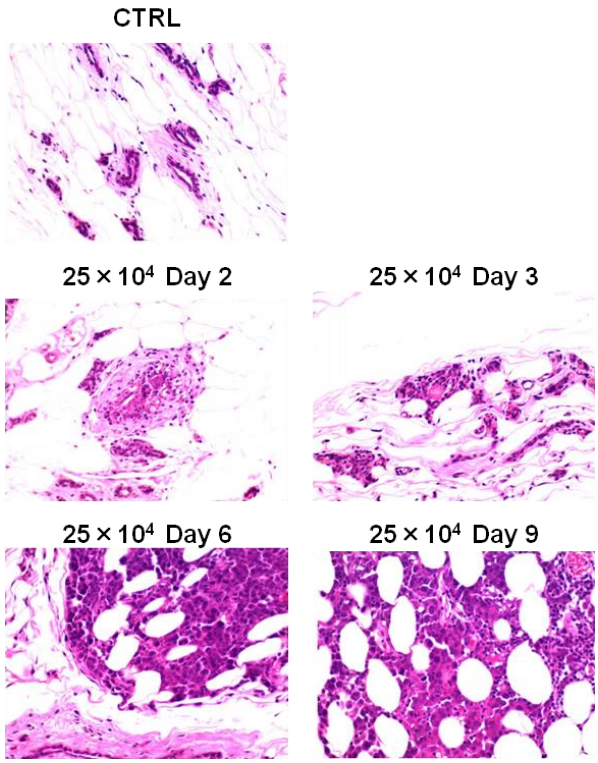

Figure 5.11. H & E staining to study early lesions in mammary ducts from F344 female retired breeders. Microscopic images were taken at ×40 objective. Thickness: 5 µ.

6 EVALUATION OF INTRADUCTAL ADMINISTRATION OF PEG DOX NANOCARRIERS FOR THE TREATMENT OF DUCTAL CARCINOMA IN SITU (DCIS)

6.1 Introduction

Ductal carcinoma in situ (DCIS), known as the most common type of non-invasive breast cancer, is the proliferation of malignant epithelial cells within the lumens of breast duct without penetrating the basement membrane [1, 2, 27-29]. The incidence had increased from 1.87 per 100, 000 women from 1973 to 1975 to 32.5 per 100,000 women in 2004 [30]. The rate of increase in incidence of DCIS has been higher than any other type of breast cancer [1]. And it has been estimated that more than 1 million women will be diagnosed with DCIS by 2020 [30]. The increased incidence is mainly attributed to the early detection by using screening mammography, which detects DCIS as microcalcifications and/or soft-tissue densities in breast [1, 31, 32]. Although it is non-invasive at this stage, DCIS has been shown to be associated with an increased risk in progression to invasive cancer based on laboratory and patient data [33-35]. Therefore intervention is required to prevent development of invasive breast cancer or local recurrence and provide significant health benefits to women [2].

DCIS is usually treated with a combination of surgery (mastectomy or lumpectomy), radiation and systemic therapies since it is really hard to distinguish the location and extent of lesions that are more likely to progress to be invasive [1, 33, 41]. There is a

general agreement that in most patients with non-multicentric DCIS, lumpectomy with postoperative breast radiation is as effective as a treatment as mastectomy with demonstrated decrease in local recurrence [35, 39, 40]. However these therapies are always associated with systemic side effects, reduced patients compliance and unnecessary expense of the health care system. Moreover, chemotherapy is not widely applied to treat DCIS because of the limited blood supply within the breast duct and the undesired adverse effects resulting from systemic administration. Several studies have reported that in human breast, there are 5 to 12 significant, non-anastomosing lactiferous ductal systems which can be approached from the openings on the nipple [53]. Moreover, there is an increasing realization that most breast cancers arise from ductal epithelial cells [2, 28, 29] and are located in a single lobe of one breast [44, 45, 52, 54]. All these suggest that intraductal approach to deliver chemotherapeutics provides an alternative opportunity in the local treatment for DCIS by targeting the carcinoma-containing lobe [27, 53].

McFarlin and Gould were the first to apply intraductal route to infuse retroviral vectors in mammary glands of rats [55]. After that the feasibility of intraductal therapy to treat breast cancer has been evaluated in several preclinical and clinical studies [56, 57, 59, 60, 100, 101]. Okugawa et al. [101] treated MNU-induced tumors intraductally with paclitaxel. And they concluded that local administration of paclitaxel might be useful for treatment of breast cancer. Love et al. [60] conducted a study in women prior to mastectomy in a phase I clinical trial, and they demonstrated the minimal toxicity of PEGylated liposomal doxorubicin (PLD) and carboplatin by intraductal administration.

This work aimed to investigate the efficacy of intraductal therapy in treating DCIS in female rats. The PEG nanocarriers were prepared by conjugating doxorubicin (DOX) with PEG polymers of different molecular weight (5, 10, 20, 40 kDa) and different structure (linear, four-arm and eight-arm) following the same synthesis scheme we used in the previous study. In this study, 5 kDa PEG-DOX and 40 kDa PEG-$(DOX)_4$ nanocarriers were selected as the candidates based on cell viability studies against 13763 Mat B III cells and mammary gland retention studies in SD female rats. The selected nanocarriers were administered into the ducts of normal F344 rats and F344 tumor model separately to investigate if there was any significant difference in nanocarrier ductal retention or DOX exposure between F344 normal rats and the F344 tumor animal model. Plasma samples were taken and pharmacokinetics of the nanocarriers were assessed. The nanocarriers were further evaluated in F344 tumor model to study the feasibility of intraductal therapy.

6.2 Materials and methods

6.2.1 Materials

Aerrane (isoflurane) was obtained from Baxter Healthcare Corporation (Deerfield, IL). The HPLC system equipped with ultraviolet (UV) and fluorescence detectors; samples were separated on the HPLC by Symmetry 300^{TM} C18 column (5.0 μm, 4.6 mm × 50 mm column) (Waters, Milford, MA). The non-invasive animal images were obtained on an

In-Vivo MS FX PRO® system from Carestream (Woodbridge, CT), and M2™ Compact High-Performance MRI (1T) system from Aspect Imaging (Toronto, Canada).

6.2.2 Cell line

The 13762 Mat B III cell line, a rat mammary adenocarcinoma cell line, was obtained from American Type Culture Collection (ATCC). Cells were maintained in RPMI 1640 medium (GIBCO/Invitrogen) supplemented with 10% fetal bovine serum and 10% penicillin (200 units/mL), and streptomycin (200 mg/mL) under condition of 5% CO_2 and 95% humidity at 37 ℃. Cells with confluence less than 90% were used.

6.2.3 Animals

Fisher 344 rats (female retired breeders) were purchased from Hilltop Lab Animals, Inc (Scottdale, PA). Rats were fed a standard diet and water *ad ilbitum*. They were housed in a room with a 12-hour light/dark cycle for at least a week before the study. All animal studies were performed in AAALAC accredited animal facilities under approved protocols from the Rutgers University Animal Use and Care Committee.

6.2.4 *In vitro* cytotoxicity studies against 13762 Mat B III cells

The cytotoxicity studies of 13762 Mat B III cells were evaluated by using Cell Counting Kit-8 (CCK-8) assay. 100 μL of cell suspension (3000 cells/well) was dispensed into a 96-well plate. 10 μL of nanocarrier solution and DOX solution with serial dilution were added to the plate. After 48 h incubation, 10 μL of CCK-8 solution was applied to each

well. The plates were incubated for 1 more hour and the UV absorbance was measured using a microplate reader at 450 nm.

6.2.5 F344 rat tumor model

The rat tumor model was established by an intraductal inoculation of 25×10^4/100 μL of 13762 Mat B III cells into the number four teat on the left side of female F344 retired breeders. On the basis of our prior experience, 2 days after inoculation of 13762 Mat B III cells were selected as the starting time point for dosing animals.

6.2.6 Mammary gland retention in female F344 normal rats and F344 rat tumor model

At day 0, the female retired breeders were anesthetized with isoflurane and placed under a surgical microscope. The number four nipple on the left side was cleaned with 70% ethanol or isopropanol. After dilation of the orifice, 13762 Mat B III cells in serum-free medium (25×10^4/100 μL) were intraductally injected into the teat using a 33 G blunt-ended needle attached to a Hamilton syringe (Hamilton, Reno, NV). At day 2, the abdominal hair and skin hair of the rats was removed. The DOX and nanocarrier solutions (0.83 mg/kg/duct DOX equivalent) were prepared in saline and injected intraductally into the left number four teat of F344 normal rats and F344 rat tumor model under surgical scope respectively (3 rats per group). Rat body images were taken by an In-Vivo MS FX PRO ® optical imaging system at different time points. Fluorescent intensity of area injected with nanocarriers or DOX was obtained by subtracting the

uninjected area. Fluorescence intensities were plotted against time and $t_{1/2}$ were estimated by non-compartmental pharmacokinetic model using PKSolver [4]. The numbers of points for terminal slope were set to auto (default). Each data point represents mean ± SD (n=3).

6.2.7 Pharmacokinetic studies

The 5 kDa PEG-DOX, 40 kDa PEG-$(DOX)_4$ and DOX (0.83 mg/kg/duct DOX equivalent concentration) were administered intraductally to F344 normal rats and F344 rat tumor model, as described in the mammary gland retention studies. Three rats were used for each group. Blood samples were collected from tail vein into the heparin-treated microtubes at predetermined time points. The whole blood was processed by microcentrifugation (2000 g for 5 min). The plasma was collected and stored at -80 ℃. Prior to analysis, the plasma samples were thawed and processed with 4 times volume of acetonitrile. The supernatant was analyzed by RP HPLC equipped with fluorescence detector (excitation wavelength is 480 nm, and emission wavelength is 590 nm). Water containing 0.1 % trifluoroacetic acid (TFA) (solvent A) and 100% acetonitrile containing 0.1% TFA (solvent B) was used as mobile phase, running the gradient from 25-80% of solvent B within 20 min. The results were normalized using DOX and nanocarrier standard curves in plasma. The maximum concentration (c_{max}) and the corresponding sampling time (t_{max}) were estimated using a non-compartmental pharmacokinetic model using PKSolver [4]. The numbers of points for terminal slope were set to auto (default). Each data point represents mean ±SD (n=3).

6.2.8 Efficacy studies in F344 tumor model

The efficacy studies were conducted after 2 days of inoculation of 13762 Mat B III cells into F344 female rats. 5 kDa PEG-DOX, 40 kDa PEG-$(DOX)_4$ and DOX were intraductally and intravenously injected separately (10 rats per group). The control group received no treatment. The dosage for each group used was 0.83 mg/kg DOX equivalent. The tumor growth and rat body weight were monitored and recorded at different days. The rats were euthanized in a CO_2 chamber when the tumor size reached the end point, which was defined as an average diameter of less than 40 mm. The tumor, liver, lung, spleen, and axillary lymph nodes were excised and fixed in 10% neutral formalin. Samples were embedded in paraffin blocks and processed for histological evaluation by routine procedures with H&E staining.

6.2.9 DOX toxicity studies

6.2.9.1 MRI images

Rat body images of F344 normal rats and F344 rat tumor model treated with PEG-DOX nanocarriers and DOX were acquired with a 1T M2^{TM} Compact High-performance MRI System (Aspect Magnet Technologies Ltd, Netanya, Israel). Two scans were taken, one covering the lower body starting at the duct, the other covering the upper torso. All scans were run at a 256-250 matrix, with the TE/TR at 80/3787 and a Flip Angle of 180 degrees. 5 averages (with each average improving the image quality) were taken each time. The data was transferred from the MRI to an analysis software program Vivoquant. In Vivoquant the images were reviewed to look for any activity (tumors or fluid, fibrosis or

irritation, metastasis). Images were compared to the prior scans (self-control) to compare growth or activity.

6.2.9.2 Histological studies

Specimens were dehydrated through a series of graded ethanol baths and then infiltrated with paraffin. The infiltrated specimens were then embedded into paraffin blocks, which were sectioned to 5-micron thickness and mounted onto glass slides. The tissue slides were stained using hematoxylin and eosin (H&E).

6.2.10 Data Analysis

Experimental values were expressed as mean±SD. nonlinear regression analysis was conducted using GraphPad Prism v.4. t_{max}, c_{max}, and $t_{1/2}$ were calculated by using non-compartmental analysis with PKSolver [4]. Survival analysis was assessed by Gehan-Breslow-Wilcoxon test.

6.3 Results and discussion

6.3.1 *In vitro* cytotoxicity studies against 13762 Mat B III cells

The *in vitro* cytotoxicity of nanocarriers was evaluated against 13762 Mat B III cell line by using CCK-8 kit. The data were fit to a sigmoidal nonlinear regression model, and the concentration at which 50% of the cells were viable (IC_{50}) was calculated on the basis of the best-fit model. As shown in Table 6.1, the IC_{50} value of DOX administered to 13762

Mat B III cells was determined to be 0.025 μM. The IC_{50} values of 5 kDa PEG-DOX, 10 kDa PEG-DOX, 20 kDa PEG-DOX, 40 kDa PEG-DOX, 40 kDa PEG-$(DOX)_4$ and 40 kDa PEG-$(DOX)_8$ nanocarriers was 0.071, 0.24, 0.76, 2.42, 0.16, and 0.15 μM separately. All were about at least 7-fold less potent than their parent drug, DOX with IC_{50} value of 0.025 μM. Therefore, the cytotoxicity of nanocarriers was reduced when DOX was conjugated to PEG polymers.

6.3.2 Mammary gland retention in female F344 normal rats and F344 rat tumor model

The mammary gland retention of nanocarriers was measured on FX-PRO imaging system. The nanocarrier solutions were administered intraductally to F344 normal rats and F344 rat tumor model, which were anesthetized at different time points to obtain whole body images (Figure 6.1). The signal intensity of free DOX decreased rapidly and became undetectable around 3 hours in F344 rats. But after PEGylation, nanocarriers showed prolonged retention in the mammary glands. Signals were obtained until 12 hours for 5 kDa PEG-DOX, while signal for 40 kDa PEG-$(DOX)_4$ reached peak in mammary gland around 12 hours after the administration.

To derive quantitative information from body images, fluorescence intensities from the injected gland were plotted against time in Figure 6.2. The mammary gland retention half-life, $t_{1/2}$, defined as the time required for fluorescence intensity to reach 50% of its peak value, was estimated from plots by non-compartmental pharmacokinetic model using PKSolver (Table 6.2). In normal rats, the $t_{1/2}$ of free DOX was estimated as

2.10±0.43 h, whereas the $t_{1/2}$ of 5 kDa PEG-DOX and 40 kDa PEG-$(DOX)_4$ was estimated as 5.87±1.19, and 14.02±1.92. In tumor model, the $t_{1/2}$ of free DOX was estimated as 3.80±1.17 h, whereas the $t_{1/2}$ of 5 kDa PEG-DOX and 40 kDa PEG-$(DOX)_4$ was estimated as 5.06±0.85 h, and 14.56±1.77 h. The results showed that DOX stayed longer time in F344 mammary gland after PEGylation. No significant difference was observed in the $t_{1/2}$ between normal rats and DCIS tumor animal model.

6.3.3 Pharmacokinetic studies

Two nanocarriers (5 kDa PEG-DOX and 40 kDa PEG-$(DOX)_4$) and DOX (control) were taken to assess the pharmacokinetic parameters (t_{max}, c_{max} and plasma $t_{1/2}$) upon intraductal administration in both F344 normal rats and F344 rat tumor model. The plasma concentration-time data in log scale (Figure 6.3). Table 6.3 listed the pharmacokinetics parameters of nanocarriers in F344 normal rats. The t_{max} for 5 kDa PEG-DOX and 40 kDa PEG-$(DOX)_4$ in normal rats were reached in 3.67±2.31 h, 26±3.46 h, respectively, but the t_{max} for DOX (control) was reached in 2±0 h only. The c_{max} for free DOX, linear 5 kDa, four-arm 40 kDa PEG DOX were 1.3e-5±4.7e-6 h, 0.014±0.0079 h, and 1.21±0.18 h respectively. In Table 6.4, the t_{max} for 5 kDa PEG-DOX and 40 kDa PEG-$(DOX)_4$ in tumor model were reached in 3.33±1.53 h, 26±3.46 h, respectively , but the t_{max} for free DOX (control) was reached in 1.17±0.29 h only. The C_{max} for DOX, 5 kDa PEG-DOX and 40 kDa PEG-$(DOX)_4$ were 2.3e-5±2.10e-5 h, 0.018±0.0010 h, and 0.55±0.29 h respectively. Thus, for both the normal rats and tumor animal model, t_{max} increased in the order: free DOX < 5 kDa PEG-DOX < 40 kDa PEG-$(DOX)_4$, similar to their order of retention in breast ducts. The C_{max} of branched 40 kDa

was higher than free DOX and linear 5kDa nanocarrier because DOX and 5 kDa PEG-DOX were eliminated from the plasma with a $t_{1/2}$ of 2.03±0.16 h, 7.36±4.67 h in normal rats and 1.64±0.45 h, 7.86±7.05 h in tumor model, but the 40 kDa PEG-$(DOX)_4$ remained longer with a $t_{1/2}$ of 44.92±6.32 h in normal rats and 48.75±8.26 h in tumor model. This is due to the fact that molecular weights of 40 kDa nanocarriers are close to the renal threshold which for globular protein is ~ 40-60 kDa, and therefore they tend to remain in the blood circulation for a longer duration. In addition, no significance between pharmacokinetic parameters generated from normal rats and tumor model was found.

6.3.4 Efficacy studies in F344 tumor model

The effects of 5 kDa PEG-DOX, 40 kDa PEG-$(DOX)_4$ and DOX on tumor volume growth are shown in Figure 6.4. No obvious rat body weight loss was observed during the treatment (Figure 6.5). The rats were euthanized once the developed mammary tumor reaching an average diameter of 40 mm. The survival curves were plotted in Figure 6.6. Statistical difference between survival curves was assessed by Gehan-Breslow-Wilcoxon test. In Table 6.5, intraductal treatment groups (DOX, 5 kDa PEG-DOX and 40 kDa PEG-$(DOX)_4$) produced remarkable significance on survival percentage at level of $p < 0.0001$, $p = 0.0002$, and $p = 0.0117$ separately rates compared to those seen in the untreated control group. However no significance was observed between the intravenous group and the untreated control. After 90 days of initial treatment, the number of rats survived was counted. As exhibited in Figure 6.7, all rats developed mammary tumors in untreated control group. The percentage of tumor free rats in intraductal treatment groups (DOX: 100%, linear 5 kDa: 88.9%, four-arm 40 kDa: 66.7%) was higher than the

intravenous group (DOX: 22.2%, linear 5 kDa: 22.2%, four-arm 40 kDa: 33.3%). All these data indicate intraductal approach is more effective in treating mammary tumors developed in F344 rats.

6.3.5 DOX affects the mammary ductal structure

MRI scanning was performed to monitor mammary tumor development upon intraductal administration of nanocarriers and DOX solution. In DOX treated group, we found soft lump developed in both normal rats and tumor model (Figure 6.8). The soft lumps had been in the mammary gland for more than 2 months, while no lumps were present in the nanocarrier treatment groups from MRI scanning (Figure 6.9). On day 65, all rats were euthanized and the mammary glands were excised for further histological studies.

Figure 6.10 shows the H & E staining of the mammary glands from normal rats and tumor animal model treated with PEG-DOX nanocarriers and DOX. Increased thickness of small arteries and veins and shrunken mammary gland ducts with a reduced number were observed in the DOX treated groups. On the other hand, normal arteries, veins and mammary gland ducts were observed in the PEG-DOX nanocarrier treated groups. Therefore DOX alters mammary ductal structure but toxicity appears to be reduced by using PEG-DOX nanocarriers.

6.4 Discussion

In breast cancer treatment, the recommended dosage for DOX is 60 to 75 mg/m^2 every 21 days by intravenous route, in the form of hydrochloride salt [3, 62]. Since systemic administration of DOX always causes undesired adverse effects, e.g. cardiotoxicity [87], a local therapy with minimized systemic exposure provides an alternative option in breast cancer treatment. In this therapy, the drug is delivered to the mammary duct directly, which apparently lead to a higher local concentration of the drug reaching to the diseased site, resulting in more potent killing of the cancerous cells in the mammary duct.

In our previous studies, the influence of molecular size and structure of PEG on DOX retention in mammary ducts of SD rats was investigated. Based on the results of cytotoxicity and ductal retention studies, we selected linear 5 kDa and four-arm 40 kDa PEG-DOX nanocarriers for efficacy studies. F344 retired breeders were used instead of SD rats to establish a breast cancer tumor model by intraductal inoculation of Mat B III cells into the mammary gland. To determine if nanocarriers follow the same molecular size dependent manner on F344 rats, ductal retention and pharmacokinetic studies were performed. Meanwhile the differences between the local and systemic pharmacokinetics of intraductally administered PEG-DOX nanocarriers and DOX alone in normal F344 and F344 tumor animal model rats were compared. Ductal retention studies using the F344 tumor animal model were performed by administering nanocarriers 2 days after the initial 13762 Mat B III cell inoculation. DOX showed a short ductal retention half-life of 2.10±0.43 h in normal F344 rats and 3.80±1.17 h in F344 tumor mode. The 5 kDa PEG DOX showed 5.87±1.19 h in normal F344 rats and 5.06±0.85 h in F344 tumor model.

The four-arm 40 kDa PEG DOX showed 14.02±1.92 h in normal F344 rats and 14.56±1.77 h in F344 tumor model. PEG DOX nanocarriers exhibited prolonged ductal retention half-lives with respect to free DOX, which was consistent with the results we obtained earlier in SD rats. There were no significant differences observed in ductal retention between the normal F344 and F344 tumor model rats.

The major aim of this study was to systematically evaluate the chemotherapeutic effects of PEG-DOX nanocarriers against DCIS mammary tumors in F344 female retired breeders. By using a well-characterized F344 tumor model, our results show that survival rates in intraductal groups were significantly improved and tumor volumes were smaller in comparison with intravenous groups. Meanwhile it was interesting to note that no tumor incidence was found in intraductal groups treated with DOX, but soft lumps were felt in the mammary glands after 3 days of intraductal injection in both normal F344 and the F344 tumor model rats. Pathology results demonstrate increased thickness of small arteries, veins and fibroblast stroma layer in the DOX treated mammary glands and also it showed reduced numbers of ducts with reduced size, suggesting that DOX affected the ductal structure. No lumps were found in the intraductal groups treated with PEG-DOX nanocarriers.

The apparent lack of toxicity due to PEGylation provides potential for translation to the treatment of early stage breast cancer in human beings. However before translation of this intraductal therapy to the clinic, there are several factors that need to be investigated including the ability to identify and cannulate the diseased ductal system, better

understanding of the anatomy of human breast and imaging methods. We performed our preclinical studies in rodents, where the anatomy of rodent breast is different from human breast. In rodent, there is only one large central duct ending at the nipple whereas in women, the number of mammary ducts is still not clear so far. Several studies have been conducted to define the number of ducts in human beings. Dated back to 1840, Cooper stated the maximum number of ducts that he was able to inject colored wax was 12 and more commonly 7-10 per nipple [43]. Teboul and Halliwell reported 5-8 ‘milk pores’ in the nipple on more than 6000 ultrasound studies of the breast ducts [48]. Moffat and Going traced 10 complete non-anastomosing ductal systems by three-dimensional computer model of a single autopsy breast [49]. Love and Barsky found an average of 5-9 ductal orifices over 200 lactating women [50]. Ramsay and colleagues described 6-12 main ducts by studied 21 lactating women with ultrasound [51]. Although controversy about the exact number still exists, all these studies suggest that there are 5 to 12 significant [53], non-anastomosing lactiferous ductal systems comprised of central ducts leading back to the chest wall and peripheral ducts draping over the central ducts, which can be approached from the openings on the nipple [27, 42, 50, 53].

Though DCIS is non-invasive lesion, it has been shown to be associated with an increase risk of subsequent invasive breast cancer [35]. The treatment is less controversial nowadays and treatment options may vary depends on the location and extent of lesions. Since the majority of DCIS does not present with palpable mass by physical examination, image-directed procedures are required for the diagnosis and treatment. However aggressive treatments with combinations of surgery (lumpectomy or mastectomy),

radiation and hormonal therapy have been used due to the inability to distinguish the lesions which are most likely to evolve into invasive disease. Although the local recurrence of DCIS and progression to invasive disease has been reduced by applying these approaches, they are associated with unwanted comorbidites including physical and emotional effects and unnecessary expense to the health care system. Based on the sick lobe theory published by Tot et al., DCIS and consequently breast carcinoma in general is a lobar disease, in which all the malignant structures (invasive, in situ, or recurrent) originate in a single lobe of one breast [44, 45, 52, 54]. And they assumed that the sick lobe is genetically malconstructed from the early embryonic life and further accumulation of genetic changes during the decades of the postnatal period may lead to malignant transformation of the epithelial cells in any part of the sick lobe [45]. Therefore excising or destroying the whole sick lobe will achieve intervention goals other than partial removal of lesions by lumpectomy. If the theory is valid, further development of advanced imaging techniques will be required to identify the sick lobe and the lesions within it. Depends on the location and extent, surgical intervention and intraductal therapy can be used to reduce the overall risk.

Here we have presented evidence that intraductal administration of PEG DOX is effective to treat mammary tumors developed in F344 tumor model with little systemic exposure. In the future, this approach may allow the use of many promising anticancer agents whose clinical application is limited due to systemic toxicity issues.

6.5 Conclusion

In summary, this work presented preclinical data supporting the effectiveness of delivering PEG DOX (linear 5 kDa and four-arm 40 kDa) intraductally in treatment of mammary tumors in F344 tumor model. Unlike DOX, no local inflammation and alteration of ductal structure in intraductal groups treated with PEG DOX nanocarriers were observed, suggesting a reduced toxicity to local ducts. In addition, we have non-invasively assessed the retention of intraductally-administered nanocarriers in both normal F344 rats and F344 tumor model. There was no significant difference of retention between normal F344 animals and F344 tumor model. The data presented here will aid in the design of further drug delivery systems for intraductal therapy to treat human DCIS.

Table 6.1. Cytotoxicity of PEG-DOX nanocarriers against 13762 Mat B III Cells

Nanocarriers and DOX	**IC_{50} (95% CI)**	**Less potent than DOX**
DOX	0.025 (0.019/0.033)	1
5 kDa PEG-DOX	0.071 (0.056 to 0.089)	2.80
10 kDa PEG-DOX	0.24 (0.15 to 0.38)	9.40
20 kDa PEG-DOX	0.76 (0.53 to 1.09)	30.04
40 kDa PEG-DOX	2.42 (1.07 to 5.49)	95.54
40 kDa PEG-$(DOX)_4$	0.16 (0.13 to 0.20)	6.32
40 kDa PEG-$(DOX)_8$	0.15 (0.11 to 0.21)	5.96

Table 6.2. Half-lives ($t_{1/2}$) of PEG-DOX nanocarriers in mammary gland of F344 normal rats and F344 rat tumor model.

PEG-DOX nanocarriers[a,b,c]	**Mammary gland $t_{1/2}$ (h, mean ±SD, n=3)**	
	F344 normal rats	F344 rat tumor model
DOX	2.10 ±0.43	3.80 ±1.17
5 kDa PEG-DOX	5.87 ±1.19	5.06 ±0.85
40 kDa PEG-$(DOX)_4$	14.02 ±1.92	14.56 ±1.77

[a] $t_{1/2}$ is defined as time at which fluorescence reaches 50% of its original value.

[b] $t_{1/2}=\ln 2/K_{el}$, where K_{el} is the elimination rate constant.

[c] K_{el} is calculated by regression of semi-logarithmic fluorescence *vs.* time data: $\ln F = \ln b - tK_{el}$.

Table 6.3. Half-lives ($t_{1/2}$) of PEG-DOX nanocarriers in plasma of F344 normal rats

PEG-DOX nanocarriers[a,b,c]	**$t_{1/2}$ (h, mean ±SD, n=3)**	**t_{max} (h, mean ±SD, n=3)**	**c_{max} (mg/ml, mean ±SD, n=3)**
DOX	2.03 ±0.16	2 ±0	1.3e-5 ±4.7e-6
5k PEG-DOX	7.36 ±4.67	3.67 ±2.31	0.014 ±0.0079
40k PEG-$(DOX)_4$	44.92 ±6.32	26 ±3.46	1.21 ±0.18

[a] $t_{1/2}$ is defined as time at which fluorescence reaches 50% of its original value.

[b] $t_{1/2}=\ln 2/K_{el}$, where K_{el} is the elimination rate constant.

[c] K_{el} is calculated by regression of semi-logarithmic fluorescence *vs.* time data: $\ln F = \ln b - tK_{el}$

Table 6.4. Half-lives ($t_{1/2}$) of PEG-DOX nanocarriers in plasma of F344 rat tumor model

PEG-DOX nanocarriers[a,b]	**$t_{1/2}$ (h, mean ±SD, n=3)**	**t_{max} (h, mean ±SD, n=3)**	**c_{max} (mg/ml, mean ±SD, n=3)**
Free DOX	1.64 ±0.45	1.17 ±0.29	2.3e-5 ±2.10e-5
5 kDa PEG-DOX	7.86 ±7.05	3.33 ±1.53	0.018 ±0.0010
40 kDa PEG-$(DOX)_4$	48.75 ±8.26	26 ±3.46	0.55 ±0.29

[a] $t_{1/2}$ is defined as time at which fluorescence reaches 50% of its original value.

[b] $t_{1/2}=\ln 2/K_{el}$, where K_{el} is the elimination rate constant.

[c] K_{el} is calculated by regression of semi-logarithmic fluorescence *vs.* time data: $\ln F = \ln b - tK_{el}$.

Table 6.5. Intraductal therapy is more effective in treating mammary tumors developed on F344 tumor model

Nanocarriers	**ID vs.CTRL**	**IV vs. CTRL**
DOX	$p<0.0001$	Not significant
5 kDa PEG-DOX	$p=0.0002$	Not significant
40 kDa PEG-$(DOX)_4$	$p=0.0117$	Not significant

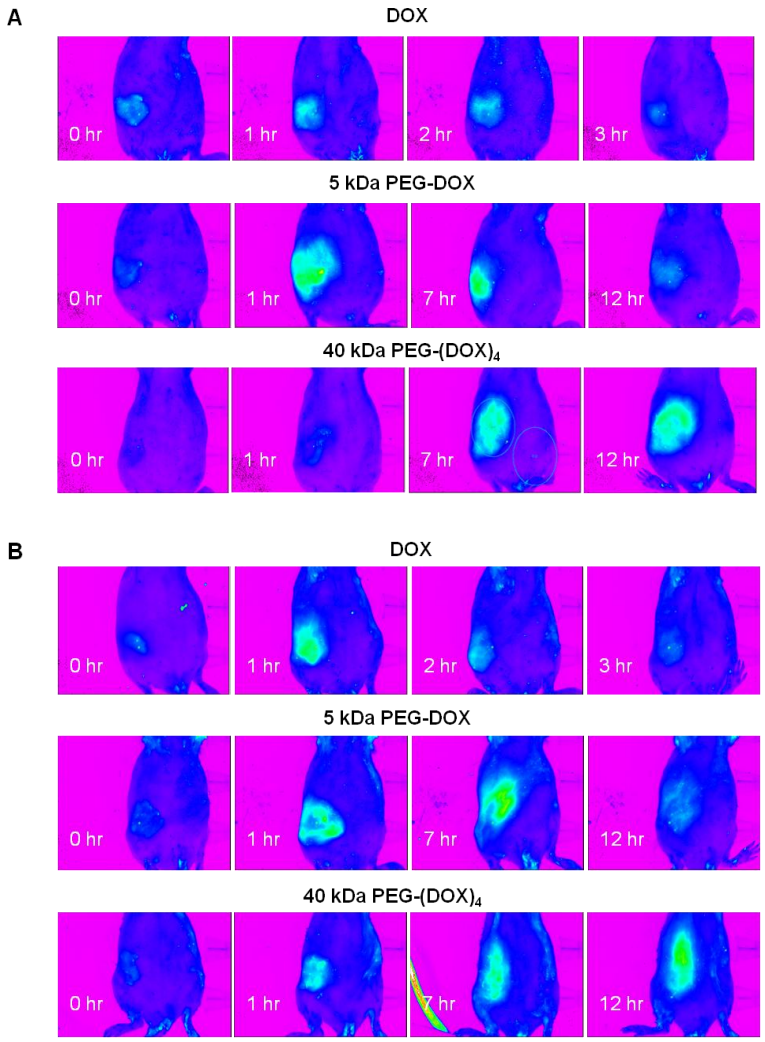

Figure 6.1. Intraductal retention of PEG-DOX nanocarriers in mammary gland: (A) F344 normal rats; (B) F344 rat tumor model. The solutions for injection (0.83 mg/kg/duct DOX equivalent) were prepared in saline and administered into the number four teat of F344 tumor model intraductally (n=3) and animals were imaged at different time points on an In-Vivo MS FX PRO ® optical imaging system.

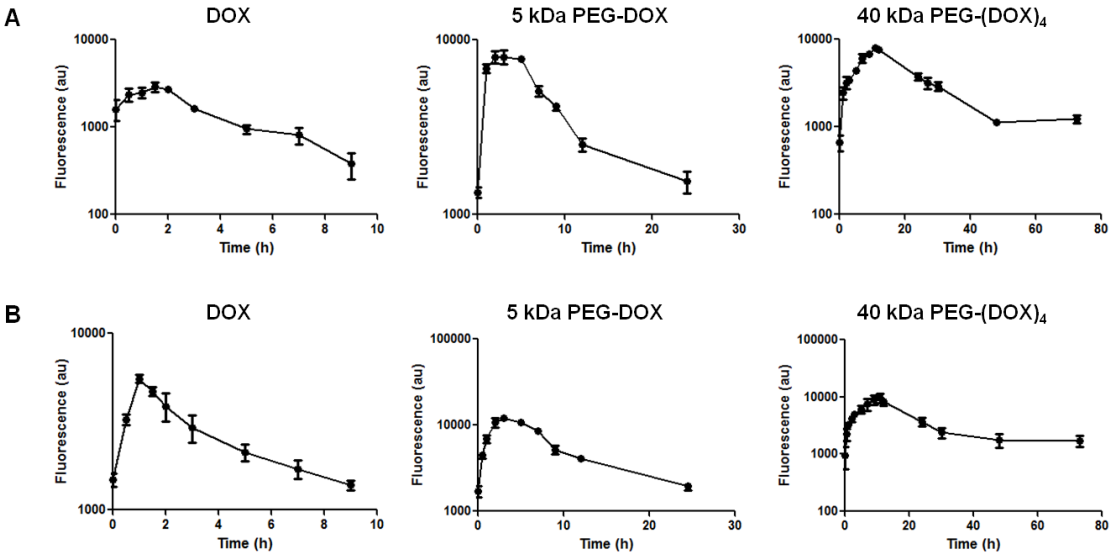

Figure 6.2. Estimation of half-lives ($t_{1/2}$) of nanocarriers in mammary gland of F344 rats: (A) F344 normal rats; (B) F344 rat tumor model. PKSolver was used to estimate $t_{1/2}$ by non-compartmental analysis, and each data point represents mean ±SD (n=3).

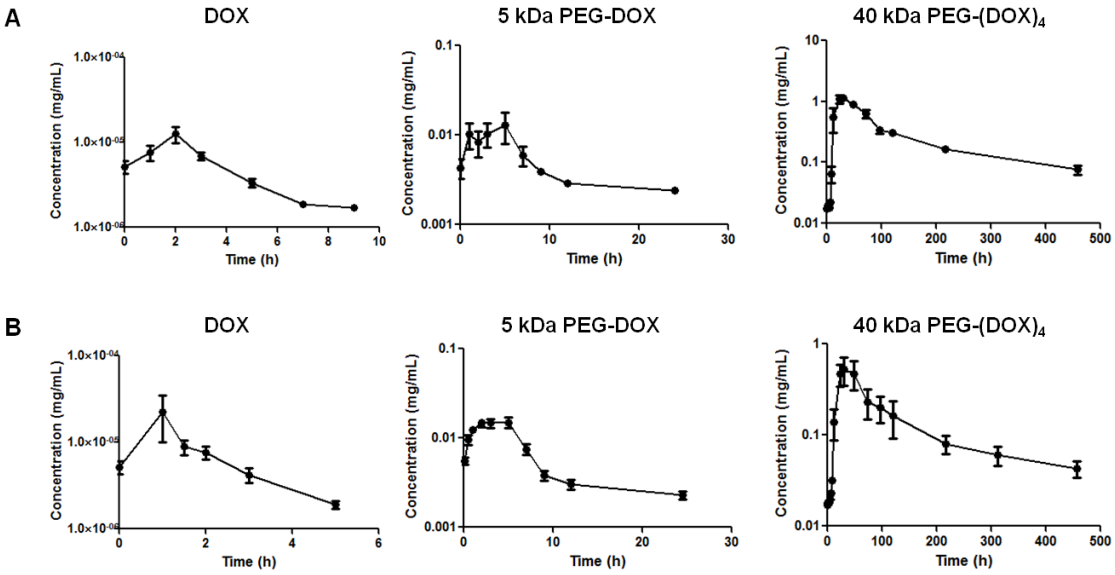

Figure 6.3. Plasma distributions of PEG-DOX nanocarriers in F344 rats: (A) F344 normal rats; (B) F344 rat tumor model. The results were normalized using DOX and nanocarrier standard curves in plasma. Each data point represents mean ±SD (n=3).

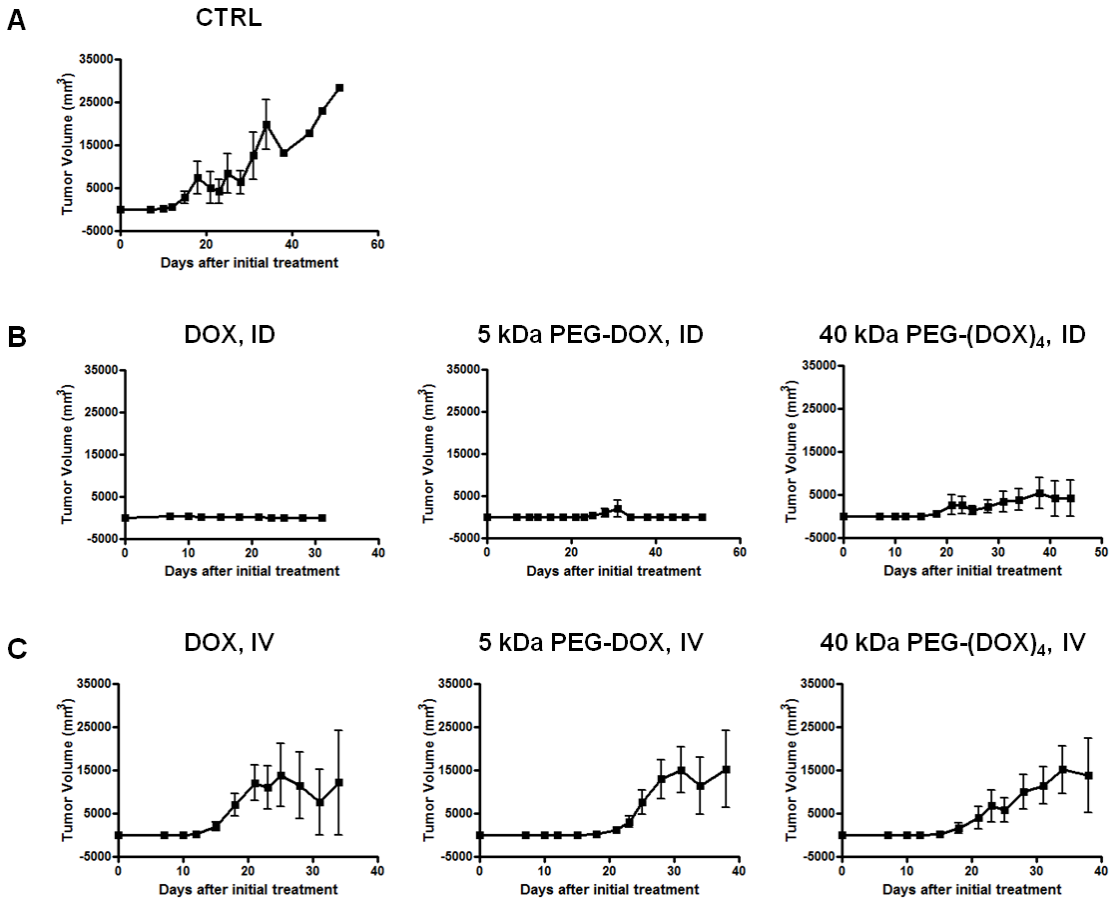

Figure 6.4. Tumor volume growth over time after the initial treatment (0.83 mg/kg/duct DOX equivalent, n=9): (A) rats with no treatment; (B) rats treated with intraductal therapy (ID); (C) rats treated with intravenous therapy (IV).

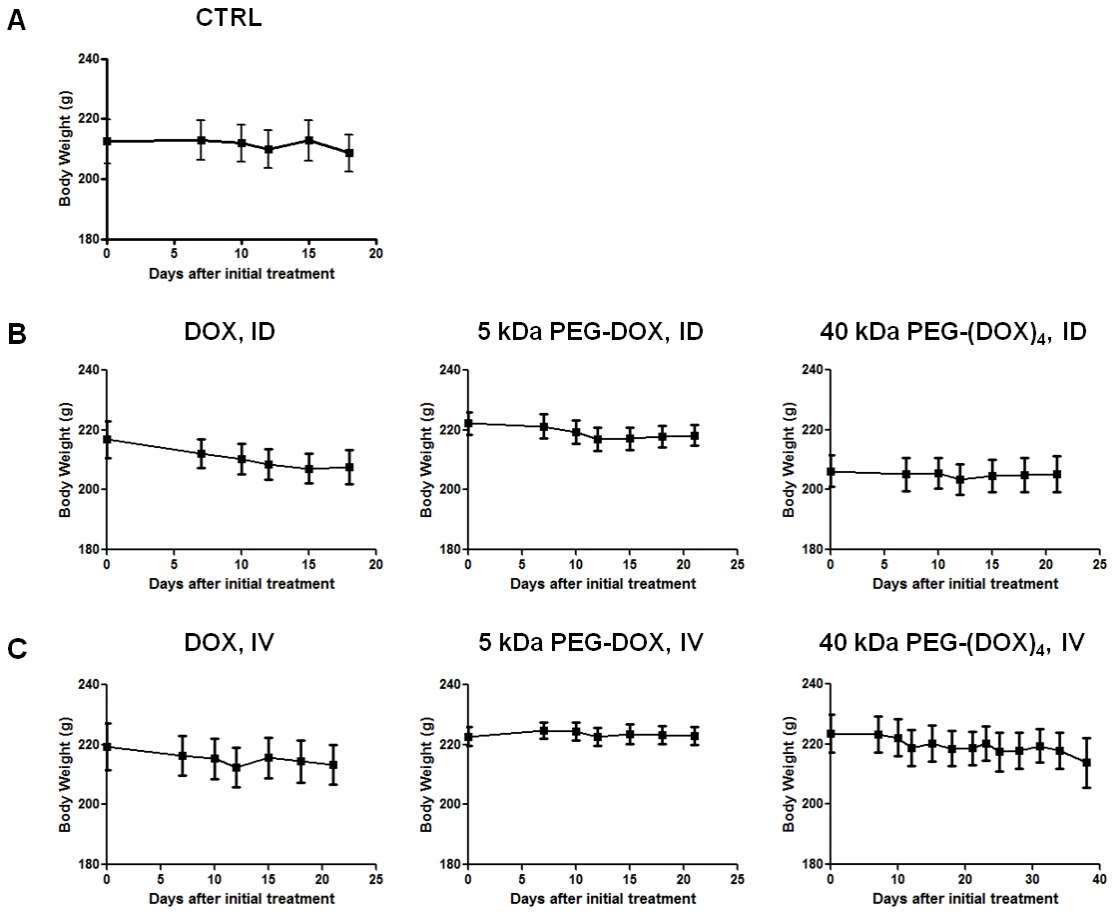

Figure 6.5. Body weight over time after the initial treatment (0.83 mg/kg/duct DOX equivalent, n=9): (A) rats with no treatment; (B) rats treated with intraductal therapy (ID); (C) rats treated with intravenous therapy (IV).

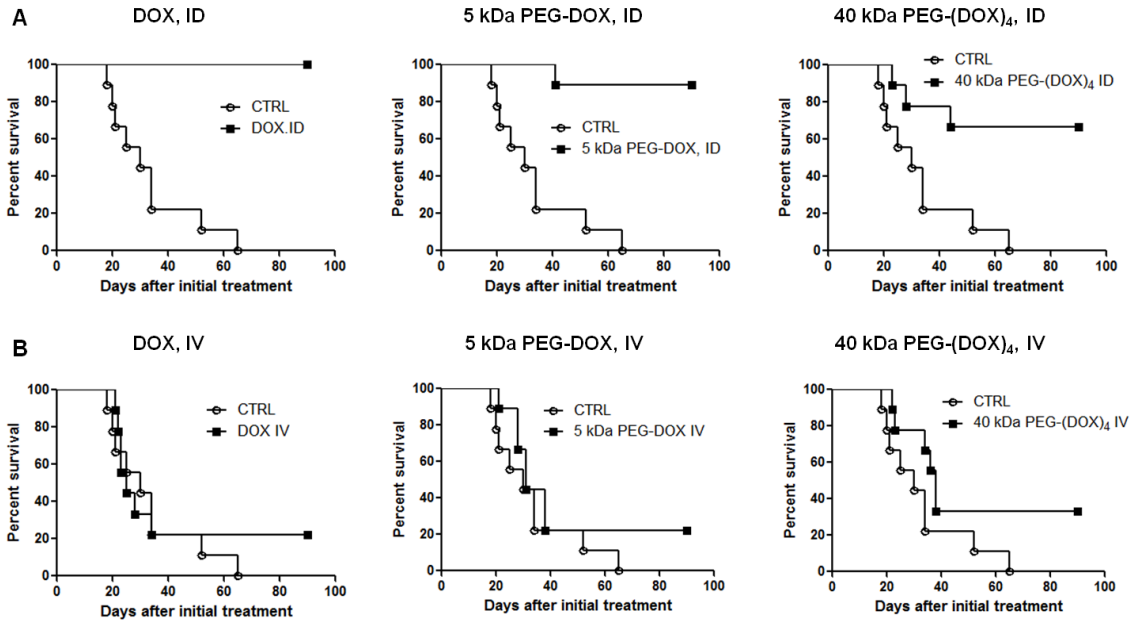

Figure 6.6. Percentage of rats survived during the studies (0.83 mg/kg/duct DOX equivalent, n=9): (A) rats treated with intraductal therapy (ID); (B) rats treated with intravenous therapy (IV). The rats were euthanized when the tumor size reached to an average diameter of 40 mm.

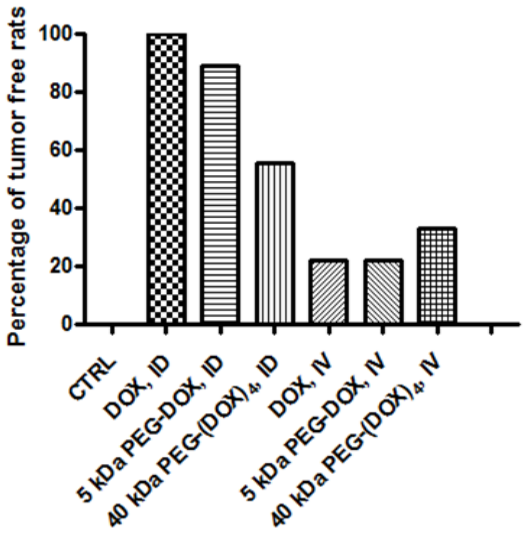

Figure 6.7. Survival percentage of F344 rats after 90 days of initial treatment.

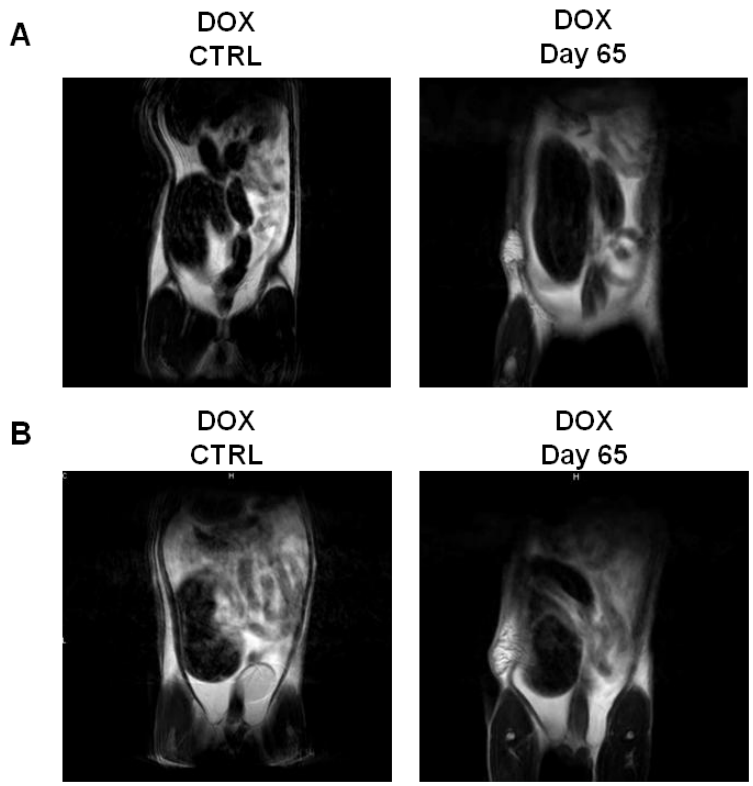

Figure 6.8. MRI scanning of mammary glands treated with DOX: (A) normal rats; (B) tumor model. The rats were treated with 0.83 mg/kg/duct of DOX and were taken for MRI images after 65 days.

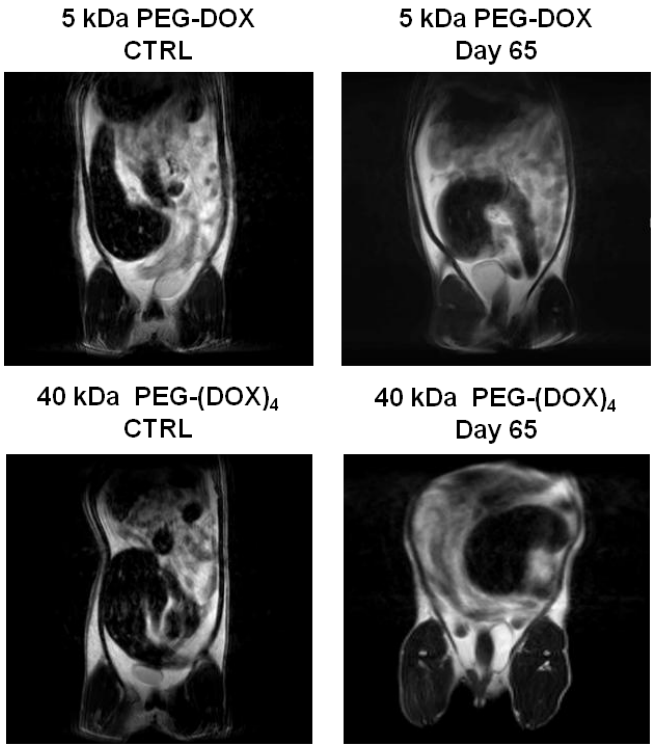

Figure 6.9. MRI scanning of mammary glands treated with PEG-DOX nanocarriers**.** The rats were treated with nanocarriers (0.83 mg/kg/duct equivalent of DOX) and were taken for MRI images after 65 days.

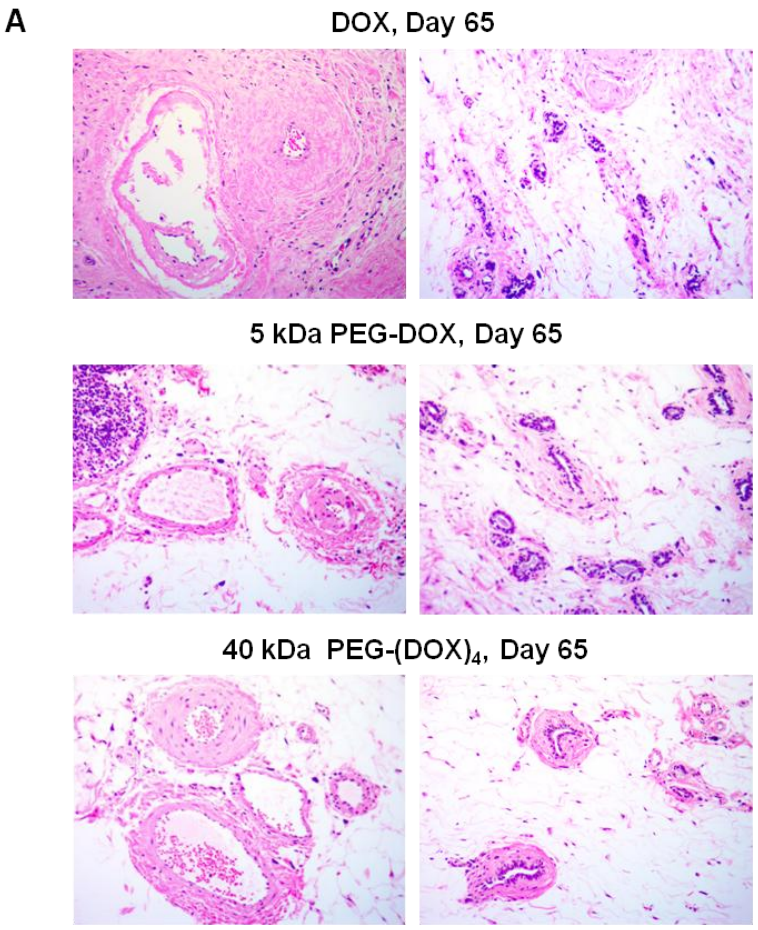
A
DOX, Day 65
5 kDa PEG-DOX, Day 65
40 kDa PEG-(DOX)4, Day 65

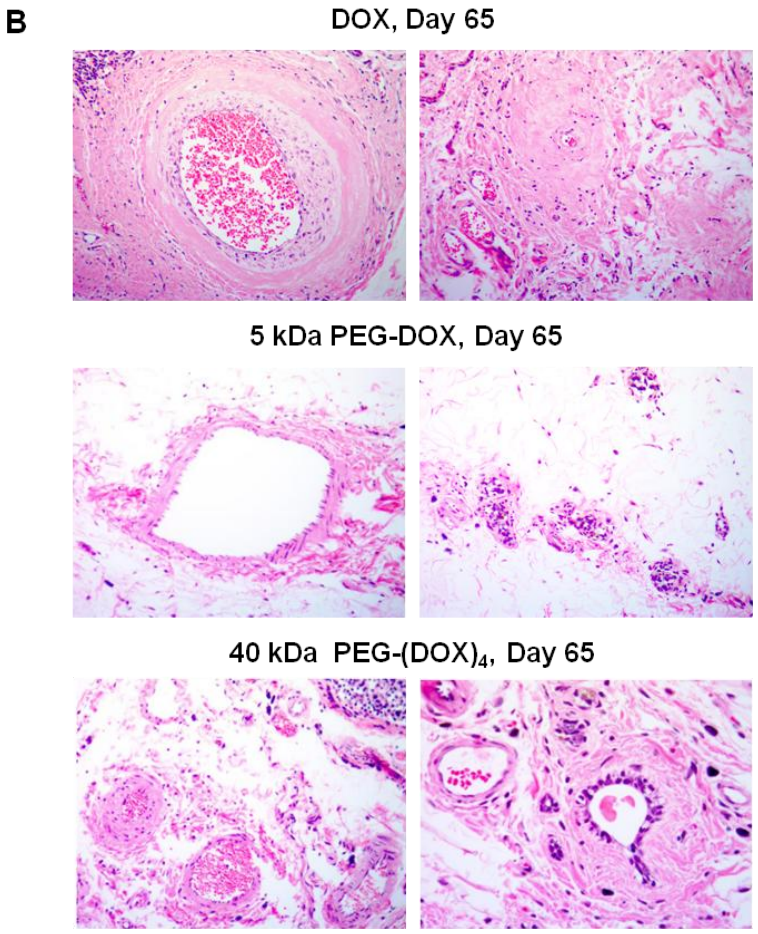

Figure 6.10. H & E staining to visualize the histology of F344 mammary ducts treated with DOX and PEG-DOX nanocarriers for 65 days: (A) normal rats; (B) tumor model. Microscopic images were taken at ×40 objective. Thickness: 5 μ.

7 SUMMARY AND CONCLUSION

Systemic administration of anti-cancer drugs has often led to undesired side effects. On the other hand, a localized therapy provides increased local drug concentration and limited systemic toxicity. Since the breast duct is accessible in animals (mice, rats and rabbits) and human, intraductal therapy to treat DCIS is promising by delivering drugs through the teat to the diseased duct.

DOX is a small molecule anti-cancer drug. It diffused out of the rat mammary gland very fast upon intraductal injection. PEGylation was used to enhance local retention of DOX in local mammary gland. This dissertation project involves design, development and evaluation of PEG DOX nanocarriers for intraductal therapy. DOX was covalently attached to PEG polymers with different molecular weight (5, 10, 20 and 40 kDa) and molecular structure (linear, four-arm and eight-arm). DOX stayed longer in rat mammary gland after PEGylation. Estimation of the retention half-lives showed the retention was influenced by both molecular weight and molecular structure of PEG. And the nanocarrier got into the blood circulation with a delayed plasma peak time when the nanocarrier had prolonged mammary gland retention. Histological studies revealed nanocarriers and DOX were able to strip the local ductal epithelium. But DOX altered the mammary ductal structure and caused inflammation in rat mammary gland while those were not observed in PEG-DOX treated groups. Thereby, PEG-DOX nanocarriers showed therapeutical effects with reduced toxicity to rat mammary gland.

A F344 tumor model was established by inoculating 13762 Mat B III cells into female F344 rat intraductally. The mammary tumor developed in a cell load and time dependent manner. It is interesting to note that young virgin rats are more susceptible to the 13762 Mat B III cell line than the retired breeders. Efficacy studies of PEG-DOX nanocarriers and DOX were evaluated on this F344 tumor model. The tumor grew slowly in all intraductal treatment groups with respect to intravenous treatment groups. Survival analysis results showed significance between intraductal group and untreated control group, while no significance was obtained when compared intravenous group and untreated control group. In summary, developed PEG-DOX nanocarriers for treatment of DCIS by intraductal approach revealed prolonged ductal retention, reduced toxicity and significance in treating F344 tumor model.

8 REFERENCES

1. Lee, R.J., et al., *Ductal carcinoma in situ of the breast.* Int J Surg Oncol, 2012. **2012**: p. 123549.
2. Burstein, H.J., et al., *Ductal carcinoma in situ of the breast.* N Engl J Med, 2004. **350**(14): p. 1430-41.
3. Fornari, F.A., et al., *Interference by doxorubicin with DNA unwinding in MCF-7 breast tumor cells.* Mol Pharmacol, 1994. **45**(4): p. 649-56.
4. Momparler, R.L., et al., *Effect of adriamycin on DNA, RNA, and protein synthesis in cell-free systems and intact cells.* Cancer Res, 1976. **36**(8): p. 2891-5.
5. Eto, Y., et al., *Development of PEGylated adenovirus vector with targeting ligand.* Int J Pharm, 2008. **354**(1-2): p. 3-8.
6. Veronese, F.M. and G. Pasut, *PEGylation, successful approach to drug delivery.* Drug Discov Today, 2005. **10**(21): p. 1451-8.
7. Thompson, H.J., M. Singh, and J. McGinley, *Classification of premalignant and malignant lesions developing in the rat mammary gland after injection of sexually immature rats with 1-methyl-1-nitrosourea.* J Mammary Gland Biol Neoplasia, 2000. **5**(2): p. 201-10.
8. Mattern, J., et al., *Human tumor xenografts as model for drug testing.* Cancer Metastasis Rev, 1988. **7**(3): p. 263-84.
9. Howard, R.B., et al., *Characterization of a highly metastatic, orthotopic lung cancer model in the nude rat.* Clin Exp Metastasis, 1999. **17**(2): p. 157-62.
10. Behbod, F., et al., *An intraductal human-in-mouse transplantation model mimics the subtypes of ductal carcinoma in situ.* Breast Cancer Res, 2009. **11**(5): p. R66.
11. Jemal, A., et al., *Global cancer statistics.* CA Cancer J Clin, 2011. **61**(2): p. 69-90.
12. Lester, J., *Breast cancer in 2007: incidence, risk assessment, and risk reduction strategies.* Clin J Oncol Nurs, 2007. **11**(5): p. 619-22.
13. Desantis, C., et al., *Breast cancer statistics, 2013.* CA Cancer J Clin, 2014. **64**(1): p. 52-62.
14. Kelsey, J.L. and M.D. Gammon, *The epidemiology of breast cancer.* CA Cancer J Clin, 1991. **41**(3): p. 146-65.
15. Hancock, S.L., M.A. Tucker, and R.T. Hoppe, *Breast cancer after treatment of Hodgkin's disease.* J Natl Cancer Inst, 1993. **85**(1): p. 25-31.
16. Kelsey, J.L. and P.L. Horn-Ross, *Breast cancer: magnitude of the problem and descriptive epidemiology.* Epidemiol Rev, 1993. **15**(1): p. 7-16.
17. Miki, Y., et al., *A strong candidate for the breast and ovarian cancer susceptibility gene BRCA1.* Science, 1994. **266**(5182): p. 66-71.
18. Sakorafas, G.H., *The management of women at high risk for the development of breast cancer: risk estimation and preventative strategies.* Cancer Treat Rev, 2003. **29**(2): p. 79-89.
19. Feuer, E.J., et al., *The lifetime risk of developing breast cancer.* J Natl Cancer Inst, 1993. **85**(11): p. 892-7.

20. Key, J., et al., *Meta-analysis of studies of alcohol and breast cancer with consideration of the methodological issues.* Cancer Causes Control, 2006. **17**(6): p. 759-70.
21. Hulka, B.S. and P.G. Moorman, *Breast cancer: hormones and other risk factors.* Maturitas, 2001. **38**(1): p. 103-13; discussion 113-6.
22. Kushi, L.H., et al., *American Cancer Society Guidelines on Nutrition and Physical Activity for cancer prevention: reducing the risk of cancer with healthy food choices and physical activity.* CA Cancer J Clin, 2006. **56**(5): p. 254-81; quiz 313-4.
23. Carter, C.L., C. Allen, and D.E. Henson, *Relation of tumor size, lymph node status, and survival in 24,740 breast cancer cases.* Cancer, 1989. **63**(1): p. 181-7.
24. Siegel, R., D. Naishadham, and A. Jemal, *Cancer statistics, 2013.* CA Cancer J Clin, 2013. **63**(1): p. 11-30.
25. Burke, W., et al., *Recommendations for follow-up care of individuals with an inherited predisposition to cancer. II. BRCA1 and BRCA2. Cancer Genetics Studies Consortium.* JAMA, 1997. **277**(12): p. 997-1003.
26. Matsen, C.B. and L.A. Neumayer, *Breast cancer: a review for the general surgeon.* JAMA Surg, 2013. **148**(10): p. 971-9.
27. Flanagan, M., S. Love, and E.S. Hwang, *Status of Intraductal Therapy for Ductal Carcinoma in Situ.* Curr Breast Cancer Rep, 2010. **2**(2): p. 75-82.
28. Peterson, J.L., et al., *Ductal carcinoma in situ of the breast.* Oncol Rev, 2009. **3**: p. 237-246.
29. Silverstein, M.J., *Ductal carcinoma in situ of the breast.* Annu Rev Med, 2000. **51**: p. 17-32.
30. Virnig, B.A., et al., *Ductal carcinoma in situ of the breast: a systematic review of incidence, treatment, and outcomes.* J Natl Cancer Inst, 2010. **102**(3): p. 170-8.
31. Ernster, V.L., et al., *Detection of ductal carcinoma in situ in women undergoing screening mammography.* J Natl Cancer Inst, 2002. **94**(20): p. 1546-54.
32. Ernster, V.L. and J. Barclay, *Increases in ductal carcinoma in situ (DCIS) of the breast in relation to mammography: a dilemma.* J Natl Cancer Inst Monogr, 1997(22): p. 151-6.
33. Leonard, G.D. and S.M. Swain, *Ductal carcinoma in situ, complexities and challenges.* J Natl Cancer Inst, 2004. **96**(12): p. 906-20.
34. Dick, A.W., et al., *Comparative effectiveness of ductal carcinoma in situ management and the roles of margins and surgeons.* J Natl Cancer Inst. **103**(2): p. 92-104.
35. Rosai, J., *Borderline epithelial lesions of the breast.* Am J Surg Pathol, 1991. **15**(3): p. 209-21.
36. Kerlikowske, K., et al., *Characteristics associated with recurrence among women with ductal carcinoma in situ treated by lumpectomy.* J Natl Cancer Inst, 2003. **95**(22): p. 1692-702.
37. Cutuli, B., et al., *Ductal carcinoma in situ of the breast results of conservative and radical treatments in 716 patients.* Eur J Cancer, 2001. **37**(18): p. 2365-72.
38. Romero, L., et al., *Outcome after invasive recurrence in patients with ductal carcinoma in situ of the breast.* Am J Surg, 2004. **188**(4): p. 371-6.

39. Talamonti, M.S., *Management of ductal carcinoma in situ.* Semin Surg Oncol, 1996. **12**(5): p. 300-13.
40. Soran, A. and V.G. Vogel, *Optimal Management of Primary Breast Cancer.* Breast J, 1999. **5**(2): p. 81-93.
41. Lagios, M.D. and M.J. Silverstein, *Ductal carcinoma in situ. The success of breast conservation therapy: a shared experience of two single institutional nonrandomized prospective studies.* Surg Oncol Clin N Am, 1997. **6**(2): p. 385-92.
42. Going, J.J. and D.F. Moffat, *Escaping from Flatland: clinical and biological aspects of human mammary duct anatomy in three dimensions.* J Pathol, 2004. **203**(1): p. 538-44.
43. Cooper, A., *On the anatomy of the breast*. London: Longman, Orme, Green, Brown and Longmans. 1840.
44. Tot, T., *DCIS, cytokeratins, and the theory of the sick lobe.* Virchows Arch, 2005. **447**(1): p. 1-8.
45. Tot, T., *The theory of the sick breast lobe and the possible consequences.* Int J Surg Pathol, 2007. **15**(4): p. 369-75.
46. Wellings, S.R., H.M. Jensen, and R.G. Marcum, *An atlas of subgross pathology of the human breast with special reference to possible precancerous lesions.* J Natl Cancer Inst, 1975. **55**(2): p. 231-73.
47. Vogel, P.M., et al., *The correlation of histologic changes in the human breast with the menstrual cycle.* Am J Pathol, 1981. **104**(1): p. 23-34.
48. Teboul, M., *A new concept in breast investigation: echo-histological acino-ductal analysis or analytic echography.* Biomed Pharmacother, 1988. **42**(4): p. 289-95.
49. Moffat, D.F. and J.J. Going, *Three dimensional anatomy of complete duct systems in human breast: pathological and developmental implications.* J Clin Pathol, 1996. **49**(1): p. 48-52.
50. Love, S.M. and S.H. Barsky, *Anatomy of the nipple and breast ducts revisited.* Cancer, 2004. **101**(9): p. 1947-57.
51. Ramsay, D.T., et al., *Anatomy of the lactating human breast redefined with ultrasound imaging.* J Anat, 2005. **206**(6): p. 525-34.
52. Ohtake, T., et al., *Intraductal extension of primary invasive breast carcinoma treated by breast-conservative surgery. Computer graphic three-dimensional reconstruction of the mammary duct-lobular systems.* Cancer, 1995. **76**(1): p. 32-45.
53. King, B.L. and S.M. Love, *The intraductal approach to the breast: raison d'etre.* Breast Cancer Res, 2006. **8**(2): p. 206.
54. Tot, T., *Correlating the ground truth of mammographic histology with the success or failure of imaging.* Technol Cancer Res Treat, 2005. **4**(1): p. 23-8.
55. McFarlin, D.R. and M.N. Gould, *Rat mammary carcinogenesis induced by in situ expression of constitutive Raf kinase activity is prevented by tethering Raf to the plasma membrane.* Carcinogenesis, 2003. **24**(6): p. 1149-53.
56. Okugawa, H., et al., *Effect of perductal paclitaxel exposure on the development of MNU-induced mammary carcinoma in female S-D rats.* Breast Cancer Res Treat, 2005. **91**(1): p. 29-34.

57. Murata, S., et al., *Ductal access for prevention and therapy of mammary tumors.* Cancer Res, 2006. **66**(2): p. 638-45.
58. Mahoney, M., Mills DJ, Love S., *Intraductal therapy of DCIS with liposomal doxorubicin: a preoperative trial.* BMC Proc, 2009. **3**: p. S31.
59. Chen, Z., et al., *Plasma concentration of doxorubicin after intraductal administration of doxorubicin long-circulating liposome in patients with breast cancer.* Chinese Pharm J, 2010. **45**(20): p. 1585-1588.
60. Love, S.M., et al., *Local drug delivery to the breast: a phase I study of breast cytotoxic agent administration prior to mastectomy.* BMC Proceedings, 2009. **3**: p. S29.
61. Minotti, G., et al., *Anthracyclines: molecular advances and pharmacologic developments in antitumor activity and cardiotoxicity.* Pharmacol Rev, 2004. **56**(2): p. 185-229.
62. Hande, K.R., *Clinical applications of anticancer drugs targeted to topoisomerase II.* Biochim Biophys Acta, 1998. **1400**(1-3): p. 173-84.
63. Frederick, C.A., et al., *Structural comparison of anticancer drug-DNA complexes: adriamycin and daunomycin.* Biochemistry, 1990. **29**(10): p. 2538-49.
64. Pigram, W.J., W. Fuller, and L.D. Hamilton, *Stereochemistry of intercalation: interaction of daunomycin with DNA.* Nat New Biol, 1972. **235**(53): p. 17-9.
65. Tewey, K.M., et al., *Adriamycin-induced DNA damage mediated by mammalian DNA topoisomerase II.* Science, 1984. **226**(4673): p. 466-8.
66. Lyu, Y.L., et al., *Topoisomerase IIbeta mediated DNA double-strand breaks: implications in doxorubicin cardiotoxicity and prevention by dexrazoxane.* Cancer Res, 2007. **67**(18): p. 8839-46.
67. Pasut, G., M. Sergi, and F.M. Veronese, *Anti-cancer PEG-enzymes: 30 years old, but still a current approach.* Adv Drug Deliv Rev, 2008. **60**(1): p. 69-78.
68. Brocchini, S., et al., *Disulfide bridge based PEGylation of proteins.* Adv Drug Deliv Rev, 2008. **60**(1): p. 3-12.
69. Abuchowski, A., et al., *Alteration of immunological properties of bovine serum albumin by covalent attachment of polyethylene glycol.* J Biol Chem, 1977. **252**(11): p. 3578-81.
70. Abuchowski, A., et al., *Effect of covalent attachment of polyethylene glycol on immunogenicity and circulating life of bovine liver catalase.* J Biol Chem, 1977. **252**(11): p. 3582-6.
71. Li, C. and S. Wallace, *Polymer-drug conjugates: recent development in clinical oncology.* Adv Drug Deliv Rev, 2008. **60**(8): p. 886-98.
72. Duncan, R., *Polymer conjugates as anticancer nanomedicines.* Nat Rev Cancer, 2006. **6**(9): p. 688-701.
73. Haag, R. and F. Kratz, *Polymer therapeutics: concepts and applications.* Angew Chem Int Ed Engl, 2006. **45**(8): p. 1198-215.
74. Harris, J.M. and R.B. Chess, *Effect of pegylation on pharmaceuticals.* Nat Rev Drug Discov, 2003. **2**(3): p. 214-21.
75. Li, W., *Current drug research on PEGylation with small molecular agents.* Progress in Polymer Science, 2013. **38**(3-4): p. 421-444.

76. Levy, Y., et al., *Adenosine deaminase deficiency with late onset of recurrent infections: response to treatment with polyethylene glycol-modified adenosine deaminase.* J Pediatr, 1988. **113**(2): p. 312-7.
77. Graham, M.L., *Pegaspargase: a review of clinical studies.* Adv Drug Deliv Rev, 2003. **55**(10): p. 1293-302.
78. Rajender Reddy, K., M.W. Modi, and S. Pedder, *Use of peginterferon alfa-2a (40 KD) (Pegasys) for the treatment of hepatitis C.* Adv Drug Deliv Rev, 2002. **54**(4): p. 571-86.
79. Bailon, P., et al., *Rational design of a potent, long-lasting form of interferon: a 40 kDa branched polyethylene glycol-conjugated interferon alpha-2a for the treatment of hepatitis C.* Bioconjug Chem, 2001. **12**(2): p. 195-202.
80. Wang, Y.S., et al., *Structural and biological characterization of pegylated recombinant interferon alpha-2b and its therapeutic implications.* Adv Drug Deliv Rev, 2002. **54**(4): p. 547-70.
81. Sundy, J.S., et al., *Reduction of plasma urate levels following treatment with multiple doses of pegloticase (polyethylene glycol-conjugated uricase) in patients with treatment-failure gout: results of a phase II randomized study.* Arthritis Rheum, 2008. **58**(9): p. 2882-91.
82. Vicent, M.J., H. Ringsdorf, and R. Duncan, *Polymer therapeutics: clinical applications and challenges for development.* Adv Drug Deliv Rev, 2009. **61**(13): p. 1117-20.
83. Sariego, J., *Breast cancer in the young patient.* Am Surg. **76**(12): p. 1397-400.
84. Meyvisch, C., *Influence of implantation site on formation of metastases.* Cancer Metastasis Rev, 1983. **2**(3): p. 295-306.
85. Volpe, J.P. and L. Milas, *Influence of tumor transplantation methods on tumor growth rate and metastatic potential of solitary tumors derived from metastases.* Clin Exp Metastasis, 1990. **8**(4): p. 381-9.
86. Octavia, Y., et al., *Doxorubicin-induced cardiomyopathy: from molecular mechanisms to therapeutic strategies.* J Mol Cell Cardiol, 2012. **52**(6): p. 1213-25.
87. Prados, J., et al., *Doxorubicin-loaded nanoparticles: new advances in breast cancer therapy.* Anticancer Agents Med Chem, 2012. **12**(9): p. 1058-70.
88. Abuchowski, A., et al., *Effect of covalent attachment of polyethylene glycol on immunogenicity and circulating life of bovine liver catalase.* The Journal of biological chemistry, 1977. **252**: p. 3582-6.
89. Flanagan, M., S. Love, and E.S. Hwang, *Status of intraductal therapy for ductal carcinoma in situ.* Curr Breast Cancer Rep, 2010. **2**: p. 75-82.
90. King, B.L. and S.M. Love, *The intraductal approach to the breast: raison d'etre.* Breast Cancer Res, 2006. **8**: p. 206.
91. Murata, S., et al., *Ductal access for prevention and therapy of mammary tumors.* Cancer research, 2006. **66**: p. 638-645.
92. Love, S.M., et al., *Local drug delivery to the breast: a phase I study of breast cytotoxic agent administration prior to mastectomy.* BMC Proceedings, 2009. **3**: p. S29.
93. Greenwald, R.B., *PEG drugs: an overview.* J Control Release, 2001. **74**(1-3): p. 159-71.

94. Isaacs, A. and J. Lindenmann, *Virus interference. I. The interferon.* Proc R Soc Lond B Biol Sci, 1957. **147**(927): p. 258-67.
95. Pfeffer, L.M., et al., *Biological properties of recombinant alpha-interferons: 40th anniversary of the discovery of interferons.* Cancer Res, 1998. **58**(12): p. 2489-99.
96. Glue, P., et al., *Pegylated interferon-alpha2b: pharmacokinetics, pharmacodynamics, safety, and preliminary efficacy data. Hepatitis C Intervention Therapy Group.* Clin Pharmacol Ther, 2000. **68**(5): p. 556-67.
97. Sundy, J.S., et al., *Reduction of plasma urate levels following treatment with multiple doses of pegloticase (polyethylene glycol-conjugated uricase) in patients with treatment-failure gout: results of a phase II randomized study.* Arthritis Rheum, 2008. **58**(9): p. 2882-91.
98. Manjula, B.N., et al., *Site-specific PEGylation of hemoglobin at Cys-93(beta): correlation between the colligative properties of the PEGylated protein and the length of the conjugated PEG chain.* Bioconjug Chem, 2003. **14**(2): p. 464-72.
99. Anderson, K.N., R.B. Schwab, and M.E. Martinez, *Reproductive risk factors and breast cancer subtypes: a review of the literature.* Breast Cancer Res Treat, 2014. **144**(1): p. 1-10.
100. Mahoney, M.E., D.J. Mills, and S. Love, *Intraductal therapy of DCIS with liposomal doxorubicin: a preoperative trial in rural California.* BMC Proceedings, 2009. **3**: p. S31.
101. Okugawa, H., et al., *Effect of perductal paclitaxel exposure on the development of MNU-induced mammary carcinoma in female S-D rats.* Breast cancer research and treatment, 2005. **91**: p. 29-34.